Weather and Climate Extremes 24 (2019) 100200

Contents lists available at ScienceDirect

Weather and Climate Extremes

journal homepage: www.elsevier.com/locate/wace

Weather situation during observed ship-icing events off the coast of Northern Norway and the Svalbard archipelago

Eirik Mikal Samuelsen[a,b,*], Rune Grand Graversen[b]

[a] MET Norway - Norwegian Meteorological Institute, P.O. Box 6314 Langnes, NO-9293, Tromsø, Norway
[b] UiT - The Arctic University of Norway, P.O. Box 6050 Langnes, NO-9037, Tromsø, Norway

ARTICLE INFO

Keywords:
Marine icing
Sea spray
Polar meteorology
Cold climate
Arctic transportation
Snow

ABSTRACT

Ship icing may lead the ship and crew in great jeopardy. Usually, predictions of such ice build-up are based on the modelling of the heat fluxes capable of freezing sea water originated from wave-ship interactions. This study, on the other hand, follows a different and more general approach by investigating the relationship between the weather situation and icing both using observed parameters from 17 ships operating in Arctic-Norwegian waters from 1980 to 2006, and by applying upper-air parameters derived from NOrwegian ReAnalysis 10 km data (NORA10). In the atmosphere, the memory aloft is larger than that near the surface providing capability of medium-range icing predictions based on such upper-air parameters. It is demonstrated that cold-air outbreak from the ice-covered ocean areas is the dominant weather situation during icing. However, around 10% of the icing events arise in cold-air outbreak mountain-wave situations with downslope windstorms near the coastlines of Northern Norway and Svalbard. It is shown that snow showers and frontal snow, mostly in combination with sea spray, increase the risk of icing. Finally, a simple model applying the temperature and temperature anomaly at 850 hPa is found to be more accurate than methods based on temperature and wind close to the surface. The model is further improved by including wind at 850 hPa.

1. Introduction

The phenomenon where either water from the atmosphere or the ocean freezes onto a ship is entitled ship icing. Ship icing may be hazardous for small vessels since it potentially leads to capsizing, submerging, and the loss of lives (Sawada, 1968; Stallabrass, 1971; Shellard, 1974; Samuelsen, 2018). Although the risk of capsizing is lower for a large ship, de-icing may be necessary in order to keep the stairways, the antennas, and the safety equipment operational (Løset et al., 2006). De-icing based on heat is energy consuming; hence avoiding icing conditions may be of interest for the ship companies also from an economical point of view (pers. comm. Kjell Are Berg-Hagen, Technical Director Tranberg AS, Member of the R. STAHL Technology Group, March 2017). Consequently, weather forecasts providing ship-icing information are valuable for operation and planning of operations of ships in a cold environment both from a safety and a financial perspective.

Traditionally, meteorologists have provided weather forecasts including icing or icing-rate severity in nowcasting or short-term prediction products. From observations or short-term prognoses of parameters like wind speed, air-temperature, and sea-surface temperature, an icing warning or forecast is issued using empirically-based methods applying the observed relationship between icing and such parameters (Sawada, 1962; Mertins, 1968; Lundqvist and Udin, 1977), or using more physically-based sea-spray icing models calculating an icing rate on a certain position of a ship from these or additional parameters like wave height (Stallabrass, 1980; Overland et al., 1986; Samuelsen et al., 2017). Details and verification of such methods are found in e.g. Samuelsen (2018). The accuracy of the short-term predictions of parameters like 10 m wind speed (V_{10m}), 2 m temperature (T_{2m}), and significant wave height (H_s) from numerical prediction models has increased during the last couple of decades (see Table 1 for definition of symbols). This accuracy enhancement includes an increased

Abbreviations: ECMWF, European Centre for Medium-Range Weather Forecasts; IFS, Integrated Forecasting System; NORA10, NOrwegian ReAnalysis 10 km data; HIRLAM, HIgh Resolution Limited Area Model; WAM, WAve Model; IQR, Interquartile range; BIAS, Mean error; MAE, Mean absolute error; OR, Odds ratio; CAO ICE, Cold-air outbreak from the ice; CAO MTW, Cold-air outbreak mountain-wave situation; NN/WS/ES, outside Northern Norway/Western Spitsbergen/Eastern Spitsbergen; v-cross, vertical cross section; PC, Percent Correct; BIASr, Bias ratio; ETS, Equitable Threat Score; HSS, Heidke Skill Score; PSS, Peirce Skill Score; I, Icing events; NI, No-icing events

* Corresponding author. MET Norway - Norwegian Meteorological Institute, P.O. Box 6314 Langnes, NO-9293, Tromsø, Norway.
E-mail addresses: eiriks@met.no, eirik.m.samuelsen@uit.no (E.M. Samuelsen), rune.graversen@uit.no (R.G. Graversen).

https://doi.org/10.1016/j.wace.2019.100200
Received 27 August 2018; Received in revised form 25 January 2019; Accepted 5 February 2019
Available online 19 February 2019

Table 1
List of symbols.

Symbol	Description
BIAS	Mean error[a]: $\frac{1}{n'}\sum_{i=1}^{n'}(P_i - O_i)$,$n'$ number of events, P_i predictions, O_i observations
C_I	Ice concentration (fraction)
c_p	Specific heat capacity of air (1004 J kg^{-1}°C^{-1})
D_D	Wind direction (°)
E_S	Total ice accumulation (cm)
$\hat{h}$	Non-dimensional mountain height
h	Mountain height (m)
H_s	Significant wave height (m)
I_S	Icing cause (code)
L_v	Latent heat of vaporisation (2.5×10^6 J kg^{-1})
MAE	Mean absolute error: $\frac{1}{n'}\sum_{i=1}^{n'}\lvert P_i - O_i\rvert$
MSLP	Air pressure at mean sea level (hPa)
N	Number of elements
N_f	Brunt-Väisälä frequency (s^{-1})
N_N	Total cloud cover (oktas)
p	Probability (fraction)
q	Specific humidity (g kg^{-1})
Q_c	Convective heat flux (W m^{-2})
Q_d	Heat flux from water droplets/solids (W m^{-2})
Q_e	Evaporative heat flux (W m^{-2})
Q_f	Heat flux released by freezing (W m^{-2})
Q_r	Radiative heat flux (W m^{-2})
R_H	Relative humidity of air (fraction)
R_S	Visually estimated icing rate (code)
SST	Sea-surface temperature (°C)
T_a	Air temperature[b] (°C)
Δt	Time difference (h)
u	Zonal wind component (m s^{-1})
U	Wind speed normal to a mountain ridge (m s^{-1})
V	Wind speed[b] (m s^{-1})
V_s	Ship speed[c] (m s^{-1})
v	Meridional wind component (m s^{-1})
W_W	Present weather (code)
w	Vertical wind component (m s^{-1})
x_i	Predictors in logistic regression model
Z	Height of pressure level(m)
β	Angle between the ship and wind[c] (°)
β_i	Coefficient in logistic regression model
Δ	Anomaly value applying monthly mean values
δ	Difference value between icing and no icing events
Φ	Geopotential (m^2 s^{-2})
ρ_a	Density of air (kg m^{-3})
Θ	Potential temperature (K)

Subscripts for variables at different altitudes	
0 m	At the surface
2 m	At 2 m height
10 m	At 10 m height
1000	At 1000 hPa
850	At 850 hPa
500	At 500 hPa

[a] Notice that bias ratio (BIASr) is a different measure applied for categorical verification (Section 2.4).
[b] At ship level if no other subscripts are applied.
[c] Calculated from position data by applying observations nearby in time ($\Delta t \leq 12$ h).

predictability of these parameters for longer forecast lead times (Richardson et al., 2013). For this reason icing warnings based on methods applying such parameters may also have gained increased predictability in the same period. However, in icing forecasts a combination of several parameters are applied, and in general predictions of a combination of parameters have larger errors compared to errors from predictions based on single parameters alone.

In addition, wave-ship interaction sea-spray icing, which is the most dangerous cause of icing (Lozowski et al. (2000); Samuelsen et al. (2015)), is a complex process having large uncertainties regarding calculations of the spray flux and the turbulent heat transfer between the atmosphere and the wetted surfaces on a ship (Samuelsen et al., 2017). Since salt is expelled from the freezing sea water during the freezing process, the freezing temperature is not directly dependent on the salinity of the incoming sea water. Mixing of the resulting salty brine water and additional fresh water from the atmosphere like snow, fog, and rain complicates the calculation of the freezing temperature and eventually icing. Thus, the accuracy of the predicted icing rates from the advanced modelling of sea-spray icing is no better than the precision to which uncertain quantities like spray flux, turbulent heat transfer, and the freezing temperature are predicted. For this reason it is unlikely that predictions of icing based on the aforementioned methods will be accurate enough to be applicable for more than a couple of days, even with increased accuracy of the numerical prediction models of today. On the other hand, upper-air weather parameters like the geopotential height of 500 hPa (Z_{500}) or the temperature at 850 hPa (T_{850}) may be predictable 16–23 days ahead in time in ensemble forecasts (Tables 2 and 3 in Buizza and Leutbecher (2015)). If simple relationships between icing and the parameters representing the weather systems on a synoptic or planetary scale are established, it might be possible to extend a forecast of potential icing risk in time relative to current methods of predicting icing.

A literature review has revealed that there were some investigations about the relationship between icing and the large-scale weather systems during the 1960s and the 1970s. Especially Sawada (1967) and Sawada (1968), and later Vasilyeva, (1971) and Borisenkov and Pchelko (1975) claim that most icing events in the seas near Japan and eastern Russia occur in the rear of the passage of low pressure weather systems bringing cold air masses from Siberia into the relatively warm ocean. All of these studies suggest a criteria of the $T_{850} \leq -18$ °C as a threshold guideline for the onset of icing. In Sawada (1967) and Vasilyeva, (1971), T_{850} and geopotential height at the same level (Z_{850}) are found to have a high correlation to icing events. In Sawada (1967) these parameters are collected from radiosonde data at a coastal station and compared with observations of icing in the sea-areas nearby. According to Sawada (1967) the application of a T_{2m}–based threshold of icing in the nomogram of Sawada (1962) has not provided satisfactory verification scores, and this study therefore suggests to use T_{850} instead. However, the relationship between these upper-air parameters and icing is only roughly evaluated in a period of one month in 1964, and no statistical analyses are applied. Borisenkov and Pchelko (1975) name this kind of forecasting procedure the ”synoptic method” without providing any details about the number of icing events analysed and the quality of the synoptic method. Other studies from the same period also focus on the synoptic conditions favourable for icing, but only in relationship with the surface parameters (Stallabrass, 1971; Shekhtman, 1971; DeAngelis, 1974). Minsk (1977) provides an overview of the different methods applied in this period including series of maps visualizing the icing potential based on climatological values of T_{2m}, V_{10m}, and sea-ice concentration (C_I). Hence, from the 1980s to present-day there has been little focus on the relationship between the weather situation and icing, and mostly on the modelling part of pure spray icing.

Longwave radiative cooling of the sea-ice cover in the Arctic ocean or of the Eurasian continent, particularly during high pressure situations with little or no clouds present, produces cold air masses during wintertime. Temperatures below −30 or −40 °C are for instance not uncommon every winter at the most extreme locations inland in Northern Norway (Norwegian Meteorological Institute, 2016). When such cold air is advected across the Barents Sea, the Norwegian Sea, and the Greenland Sea, extensive heat exchange is taking place between the atmosphere and the ocean due to the large temperature differences across the interface of those two media. Such cold surges are often entitled cold-air outbreaks or marine cold-air outbreaks in the literature (e.g. Kolstad (2017) or Papritz and Spengler (2017)). Due to the northward transportation of warm water from the North Atlantic Current, surface sensible and latent heat fluxes may in some areas reach values above 500 W m^{-2} according to observations and model

calculations (Papritz and Spengler (2017) and references therein). Cold-air outbreaks from the ice (CAO_ICE) are often associated with deep convection downstream resulting in possible development of polar lows (Kolstad, 2011), throughs, or more isolated snow showers, i.e. phenomena favourable for icing since they are providing relatively strong winds, high waves, and low temperatures in already sub-freezing conditions (Samuelsen, 2018). At the same time there might also be other parameters increasing the risk of icing. For instance Brown and Roebber (1985) and Brown and Agnew (1985) emphasize that spray icing and snow frequently occur simultaneously during cold-air outbreaks, but it is not clear whether the snow by itself increases the icing risk or whether the snow is just a consequence of a weather situation providing convection generated by the cold-air outbreak.

On the contrary, cold-air outbreaks from the land areas of Northern Norway and the Svalbard archipelago are often affected by the terrain with steep mountains going from the sea level up to elevations of about 500–1,500 m (maximum 1,915 m above sea level) (Samuelsen, 2007; Skeie and Grønås, 2000). Since the air masses upstream are strongly stratified in such weather conditions, these cold-air outbreaks will interact with the terrain leading to mountain waves (CAO_MTW) which are often associated with downslope windstorms on the lee-side of the barriers in conjunction with gap flows downstream of the long and relatively wide fjords. Adiabatic warming due to the descending air on the lee-side of the mountains enhances stability downstream of these barriers, and this may result in shallower convection giving a potential for less intense showers in the CAO_MTW events compared to the CAO_ICE events. This is therefore a strong argument for separating between these two types of cold-air outbreak weather situations. Samuelsen et al. (2017) indicate that there might be some association between icing events and CAO_ICE events, since most of the events documented in this study occurred when a low-pressure system was located in the eastern part of the Barents Sea with a corresponding northerly flow from the ice further to the west (Supplementary material in Samuelsen et al. (2017)). In addition, Samuelsen et al. (2015) analyse the strongest icing event ever documented for the coast guard vessel type called ”KV Nordkapp”, pinpointing that it arose during a strong CAO_ICE with the development of a violent polar-low storm. However, CAO_MTW events have not been directly associated to icing events in earlier studies. Nevertheless, recent investigations of ship incidents in Norway (Norwegian Maritime Authority, 2014) combined with information from reanalysis data, show that the last disastrous icing event with human causalities in Northern Norway occurred in a CAO_MTW event in 1999 (Supporting information Fig. S1).

While the Samuelsen et al. (2017) study focuses on icing observations and icing modelling for more detailed icing-rate verification purposes, the current study follows a more general approach by comparing the weather conditions during icing and no-icing events, and these conditions compared to climatology. More than 1,500 ship observations from the Norwegian Meteorological Insitute collected in the period 1980–2006 are dichotomized in icing and no-icing events according to information from the observers. Furthermore, reanalysis data of important parameters are derived for 801 of these cases, both aloft and near the surface, from the NOrwegian ReAnalysis 10 km data (NORA10); a hindcast of parameters from a HIgh Resolution Limited Area Model (HIRLAM) from Northern Europe with approximately 10 km horizontal resolution including a WAve Model (WAM) with a similar horizontal resolution (Reistad et al., 2011). Simple logistic regression models are applied on a pre-selected training data set in order to design a possible forecasting method from the upper-air parameters for application in medium-range predictions of icing. These simplified statistical models of the upper-air parameters from NORA10 are verified together with some of the commonly-applied methods using thresholds for the surface parameters T_{2m} and V_{10m} against a pre-selected control group.

There are three main goals of the paper:

(1) Determining the weather parameters important for ship icing using observations for several ship types, which is based on a much larger data set compared to that applied in Samuelsen et al. (2017) and Samuelsen (2018).
(2) Investigating large-scale weather situations in which icing events develop and situations for which no icing is reported.
(3) By following the results of these two investigations, develop a simple model for medium-range icing predictions.

Section 2 presents some background on icing, icing observations, reanalysis, and regression model. Section 3 analyses the importance of various weather parameters in icing versus no-icing events, using both the observations from the current study and from the study of Vasilyeva, (1971). Section 4 presents the most common weather situations that the selected icing and no-icing events are reported in. This is done by analysing horizontal map composites, vertical profiles, and vertical cross sections utilizing NORA10 data in both CAO_ICE and CAO_MTW events. Finally, Section 5 presents verification results from the logistic regression model developed using upper-air parameters compared with verification results obtained from methods using surface parameters alone.

2. Theory and methodology

2.1. Marine-icing theory

Marine icing is a complex phenomenon in which many processes are involved. For this reason only a brief review relevant for the current study is summarized in the following section. For more details the reader is referred to e.g. Horjen (1990); Lozowski et al. (2000); Kulyakhtin (2014); Samuelsen et al. (2017). The main focus in these papers is on the modelling part of sea-spray icing.

Freezing of water on a ship is dependent on the flux of water from the ocean and the atmosphere, and the heat exchanged between the surroundings and this water available for freezing. For wave-ship-collision sea-spray icing, the following heat balance with the most important heat fluxes is normally applied (Lozowski et al., 2000; Samuelsen et al., 2017; Samuelsen, 2018):

$$Q_f = Q_c + Q_e + Q_d + Q_r \quad (1)$$

The heat released during the freezing process (Q_f) is in Eq. (1) balanced by three major heat fluxes from the atmosphere, i.e convective/sensible heat flux (Q_c), evaporative/latent heat flux (Q_e), and radiative heat flux (Q_r), and heat exchanged by contact between the freezing water surface and some additional water from either the atmosphere or the ocean (Q_d). Since the turbulent fluxes Q_c and Q_e are the most important cooling terms (Samuelsen et al., 2017; Samuelsen, 2018), turbulent conditions characterized by higher fluctuations of wind, humidity, and temperature will lead to more cooling than in more quiet conditions.

2.2. Icing data selection

A comprehensive inspection of the climate database of the Norwegian Meteorological Institute revealed icing observations from 17 different ships in the period 1980 to 2006 during the winter season lasting from September until May. Most of these ships are coast guard vessels with a length of about 50–100 m. These ships have provided observations of weather and ocean parameters regularly when operating in the seas around Northern Norway and the Svalbard archipelago in this period (Fig. 1).

Icing observations are collected with a subjective estimate of whether the ice is accumulating or not (R_S), the cause of icing (I_S), and the total ice thickness registered at the time of the observation (E_S). Samuelsen et al. (2017) applied two E_S-observations nearby in time to derive an estimate of the icing rate from the KV Nordkapp ships. In the current study it is decided to utilize the R_S-observations for information about icing or no-icing at the time of the observation. However, it is not distinguishable whether missing icing information from some months or years in the time period studied is either due to the lack of particular icing weather situation, reduced operations, or missing/forgotten icing

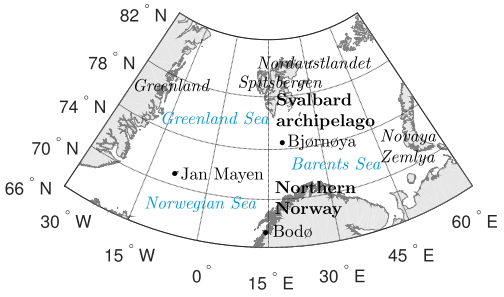

Fig. 1. Overview of some geographical names in the area of the ship observations applied in the current study. The positions of the radiosonde stations at Bjørnøya, Jan Mayen, and Bodø applied in the verification of some upper-air parameters are marked with dots, seas are marked with blue italic print, major islands are marked with black italic print, and the approximate position of important regions are marked with black boldface print. (For interpretation of the references to colour in this figure legend, the reader is referred to the Web version of this article.)

reports during completed operations. For this reason it is not possible to study the inter-annual or inter-monthly frequency of icing versus no icing in the current study. Another consequence of this lack of information is that it is uncertain whether events that do not register information about R_S truly are cases with no ice accumulation. Thus, no-icing events selected with the basis in the R_S-parameter may occur in weather situations quite similar to those of the icing events, since in these no-icing events, icing may have been encountered a short period before, or a short period after the no-icing events. Further detailing about the selection process of the icing and no-icing events can be found in the Supporting information (Section S.1).

The final data set with the dichotomized icing data may be seen in Fig. 2. This figure also includes all observations from ships in the database inside the same area in the years 1980–2006. Monthly mean values from the ship observations are calculated inside each of the 20 latitudinal-longitudinal grid boxes visualized in Fig. 2.

2.3. Reanalysis data

Reanalysis data are derived from NORA10 at the same junctures as the icing and no-icing events. NORA10 is a downscaling of ERA-40

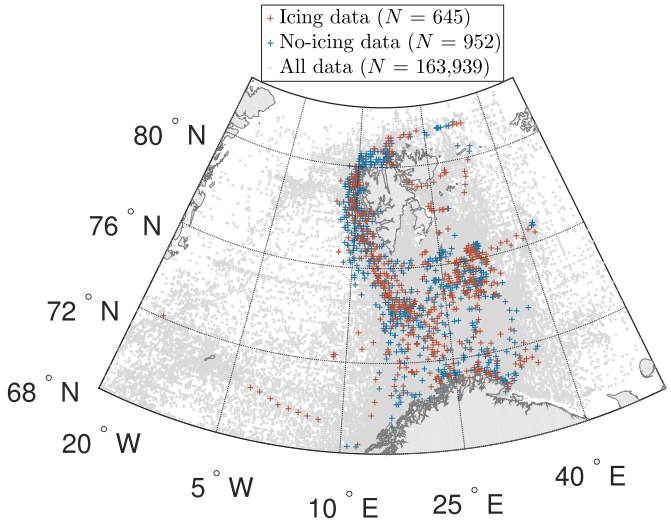

Fig. 2. Map of all icing (red crosses) and no-icing events (blue crosses) applied in the current study. In addition, all ship observations in the years 1980–2006 are plotted (small grey crosses) between the latitudes 68 °N and 82 °N, and the longitudes 20 °W and 50 °E. (For interpretation of the references to colour in this figure legend, the reader is referred to the Web version of this article.)

(Uppala et al., 2005) from 1958 to 2002. After the year 2002 the operational analyses from European Centre for Medium-Range Weather Forecasts Integrated Forecasting System (ECMWF IFS) is applied. The downscaling is performed over the Northern Atlantic with the HIRLAM version 6.4.2 (Undén et al., 2011) set up on a rotated grid with approximately 0.1 ° resolution (Furevik and Haakenstad, 2012). The WAve Model (WAM) (The Wamdi Group, 1988) is forced from HIRLAM on the same grid. As described in Samuelsen et al. (2017) there are in icing situations small differences in the temperature and wind-speed errors relative to ship observations between the NORA10 downscaled with ERA-40 compared to a version of NORA10 downscaled with ERA-Interim (Dee et al., 2011). The former is here applied since the WAM model has not been run with HIRLAM downscaled from ERA-Interim. More details about NORA10 including a figure of the HIRLAM and WAM domains may be found in Reistad et al. (2011).

The ship observations are usually recorded every 3 h during an expedition, and after the year 2005 there are also observations recorded every hour. However, upper-air parameters like T_{850} are only available every 6 h in the NORA10, and consequently analyses applying these parameters may only be conducted with those observations occurring at 0000, 0600, 1200 and 1800 UTC. Hence, when applying NORA10 upper-air parameters the amounts of events applied are reduced from 645 to 333 icing events, and from 952 to 468 no-icing events. Climatological values of the NORA10 parameters are derived by calculating the monthly average values for all of the relevant atmospheric parameters in the years 1980–2006. Anomaly values are then calculated by subtracting these mean monthly values from the values in the icing or no-icing events occurring in the same month (anomaly = events − climate). Each icing or no icing observation has a different spatial and temporal position, and reanalysis data are derived for all these events. However, when investigating the events in connection with the large scale weather systems, it is discovered that there are some of the observations occurring at the same juncture but at a different location in conjunction with the same low or high pressure system. There are also observations occurring nearby in time, but still with reference to the same weather system. As a consequence it is possible to calculate the average weather in icing or no-icing events in two different manners: Firstly, one may consider all observations independently, meaning that a single low pressure system with a certain cold air mass in the rear of it, connected to more than one icing observation, is counted several times. The average weather is then calculated as the mean value of the parameters derived from NORA10 for each of the 333 icing events or the 468 no-icing events inside the same area. Secondly, it is possible to cluster icing or no-icing events arising from the same weather system before calculating the final average value. A simple clustering technique is applied by connecting all icing events taking place consecutively in time with time differences less than 18 h between each junctures. The same procedure is applied for the no-icing events. For each of the clusters the mean value of the parameters is calculated. The icing events are then consolidated into 166 clusters, while the number of clusters for the merged no-icing events is 183. This latter method is applied when calculating the average weather for all icing and no-icing events inside the same area of interest, and comparing this average weather with climatological values. However, when statistically investigating the values of a single upper-air or lower-air parameter in connection with a particular icing or no-icing event, all events are treated separately. In such a context the particular upper-air or lower-air value in itself is of interest, including its association to the icing/no icing event, but not the weather system this event is connected to.

The atmospheric part of NORA10 includes 40 model levels from the top of the atmosphere to the surface with higher vertical resolution in the lowest part of the atmosphere compared to the upper. These model levels are interpolated to pressure levels in the lowest part of the atmosphere namely every 25 hPa between 1000 and 850 hPa, every 50 hPa from 850 to 500 hPa, and every 100 hPa from 500 to 300 hPa. In order to investigate different weather patterns in conjunction with the icing and no icing events, vertical temperature profiles and vertical

cross sections are calculated from these interpolated pressure levels. The cross sections are constructed to follow the main wind direction in three weather-situation categories evaluated. For each of the weather situations considered, the average values are calculated from the different parameters following constant latitudes or longitudes corresponding to the interval of latitudinal or longitudinal positions of the observed icing and no-icing events (Section 4.2).

2.4. Development and verification of a simple icing-warning model

Since the degree of icing is not a part of the applied data, there are only two outcomes of icing: icing or no-icing. Accordingly logistic regression is applied instead of linear regression in order to investigate the importance of different predictor variables. A logistic regression model with several predictors may be constructed as follows (see e.g. Ch. 5 in Vittinghoff et al. (2011)):

$$\log\frac{p(x_i)}{1-p(x_i)} = \beta_0 + \beta_1 x_1 + \ldots + \beta_i x_i \quad (2)$$

$$\mathrm{OR}_i = \exp\beta_i \quad (3)$$

Such a model is constructed to provide the probability ($p(x_i)$) of icing occurring (or no icing ($1-p(x_i)$)) assuming that there is a linear relationship between the logarithm of the odds ($p(x_i)/(1-p(x_i))$) of icing and the predictor x_i from the data set. The predictors may be both continuous and categorical. A major assumption in the logistic regression model is the requirement of independence between the values of each outcome. Since a particular observation of icing or no-icing is recorded at a different location spatially or temporally compared to the other observations of icing or no icing, and is tested according to the local recorded or derived predictor values at that exact location, it is assumed that the event being icing or no icing is independent of the next or previous event. The possible autocorrelation between the icing events occurring in conjunction with the same weather system are then not taken into account. The odds ratio (OR_i) for a given predictor variable (x_i) is defined as the ratio between the odds of this predictor variable with 1 unit higher value, $p(x_i+1)/(1-p(x_i+1))$, and the odds of this predictor variable with the initial value, $p(x_i)/(1-p(x_i))$, holding all other variables constant. This is easily calculated by applying the coefficients (β_i) in the logistic regression model (Eq. (3)). For a dichotomized categorical predictor variable in which the x_i-value is either one or zero, the OR indicates the increased risk of icing associated with the inclusion of this parameter based on the data set.

In order to derive a simple model that is easily adoptable for different users, dichotomized predictors of some upper-air parameters above or below certain thresholds are applied in such a logistic regression model (Eq. (2)). Furthermore, the 801 icing and no-icing events are divided into a training data set which is applied during the model-selection process, and a control data set which is used to verify the models. The data are divided into the two categories based on the day of the month that the observation was recorded. The training data apply all observations recorded after the 10th in a month, and the control data apply the other observations. This procedure approximately divides the data in parts of 2/3 and 1/3 with 261 observations in the control data set in which 97 are icing events. The models are only evaluated against reanalysis data, and not data from medium-range prediction models. However, it is assumed that the predictions of the upper-air parameters are more accurate in the medium range, i.e. more than a couple of days or a week, than the surface parameters are (Haiden et al., 2016).

Furthermore, observed and predicted icing and no-icing events are divided into 2×2 contingency tables representing the four entries: hits (observed and predicted icing), misses (observed, but not predicted icing), false alarms (predicted, but not observed icing) and correct negatives (predicted and observed no icing). From such a table it is possible to calculate several verification scores. It is decided to apply the following five scores: Percent Correct (PC), Bias ratio (BIASr), Equitable Threat Score (ETS), Heidke Skill Score (HSS), and Peirce Skill Score (PSS). PC, HSS, and PSS are described in a detailed manner in Samuelsen et al. (2017) for 4×4 contingency tables, and in short these are measures taking into account the number of hits and correct negatives relative to the total number of events with or without adjustments for those hits occurring due to random chance. The BIASr provides the ratio of the total number of predicted icing events relative to the observed number of icing events regardless of hits. The ETS is a score measuring the fraction of observed and predicted icing events that are correctly forecasted (hits) without considering the correct negatives (threat score) with an additional adjustment for those hits occurring due to random chance (equitable threat score). The ETS, HSS, and PSS are all equitable. More details of the calculation procedure of all these scores are provided e.g. by Ch. 8 in Wilks (2011).

3. Parameters related to icing

3.1. A comparison with Vasilyeva (1971)–study

Vasilyeva, (1971) presents an overview of the frequency of occurrence of icing events in relationship with different intervals or above or below certain thresholds for some observed values of surface atmosphere and ocean parameters regarded as important for icing. These observations are recorded on fishing boats operating in the years 1965–1970 in several sea areas around the world. It is therefore interesting to compare these findings from the Barents Sea and the Norwegian Sea with the observations of the current study (Table 2). More details about the construction of this table is described in the Supporting Information (Section S.2).

In general the icing events of the current study relative to Vasilyeva, (1971) have higher waves, stronger winds, and lower air temperatures (Table 2). This may indicate that icing for fishing boats may occur under less severe conditions than the icing events of the larger ships of the present study. In addition, it may indicate that these larger ships are operating in areas with more severe condition than the fishing vessels. Finally, it may also indicate different weather situations from the six-year period of 1965–1970, compared to the 27-year period of 1980–2006. It is intriguing to notice that icing in conjunction with winds from around the south (from 90 to 270 °) are more dominating in the Vasilyeva, (1971)–study, while in the current study icing situations with winds from around the north (270–90 °) are the dominating ones. In general winds from the north in these sea areas are associated with CAO_ICE conditions. On the contrary winds from around the south along with icing mostly arise when the winds are blowing from the cold land areas of the European continent, i.e. CAO_MTW conditions. However, it is not possible from this description alone to conclude whether the difference between the data sets is due to differences in ship type or to the weather situations between the years. It might as well be an effect of both circumstances. It is also observable that for all winter or summer data the frequency of occurrence in the different wind-direction quadrants are quite similar, with a slight dominance of southerly winds in winter and northerly winds in summer.

3.2. Observed parameters in icing verus no-icing events

In general, Table 2 indicates clear differences between the icing and no-icing events. Higher waves and stronger winds are the most prominent signatures in the icing relative to the no-icing events. This is further underlined in Fig. 3 where the data are summarized with box plots for some of the same parameters. From this figure there is a strong indication that when comparing air-temperature between the icing and no-icing events, the median values in the two categories are not significantly different. This is observed by comparing the so-called notches or 95% confidence intervals around the medians of the two groups for this particular parameter. Since the notches do overlap for the median

Table 2
The frequency of occurrence of icing events and other events in a selected interval above or below certain thresholds of some values of surface atmosphere and ocean parameters regarded as important for icing. The structure of the table is derived from Vasilyeva, (1971) which presents icing events from fishing boats in the years 1965–1970. Only those events recorded from the Barents Sea and the Norwegian Sea are presented in this table, as well as the icing events, no-icing events, all winter events[b], and all summer events[b] of the ships in the current study recorded in a similar region in the years 1980–2006 (Figs. 1 and 2). The frequency of occurrence in a selected interval for a certain category is provided as a fraction of the total number of events (*N*) in the same category. *N* is presented in the rightmost column. More details about the construction of this table is described in the Supporting information (Section S.2).

		Wave height (m)						*N*
		0	⟨0,1]	⟨1,3]	>3			
Vasilyeva, (1971)	Icing	–	–	0.81	0.19			871
Current paper	Icing	0.00[a]	0.02	0.39	0.58			626
	No-icing	0.07	0.09	0.57	0.26			902
	All winter data[b]	0.03	0.09	0.61	0.26			96,705
	All summer data[c]	0.09	0.17	0.65	0.09			53,451
		Wind speed (m s^{-1})						*N*
		0	⟨0,10]	>10				
Vasilyeva, (1971)	Icing	–	0.32	0.68				953
Current paper	Icing	0	0.19	0.81				645
	No-icing	0.00[a]	0.48	0.52				951
	All winter data[b]	0.02	0.61	0.38				110,824
	All summer data[c]	0.05	0.79	0.16				65,447
		Wind direction (°)						*N*
		0	⟨0,90]	⟨90,180]	⟨180,270]	⟨270,360]		
Vasilyeva, (1971)	Icing	–	0.29	0.30	0.22	0.19		953
Current paper	Icing	0	0.46	0.11	0.03	0.40		645
	No-icing	0.00[a]	0.39	0.22	0.12	0.27		951
	All winter data[b]	0.02	0.23	0.25	0.27	0.24		110,696
	All summer data[c]	0.05	0.25	0.23	0.22	0.25		65,301
		Air temperature (°C)						*N*
		< − 20.0	[−20.0, −15.0⟩	[−15.0, −10.0⟩	[−10.0, −4.0⟩	[−4.0, 0.0⟩	≥ 0.0	
Vasilyeva, (1971)	Icing	–	0.02	0.16	0.67	0.15	–	966
Current paper	Icing	0.01	0.09	0.26	0.54	0.09	0	645
	No-icing	0.02	0.08	0.28	0.40	0.19	0.03	907
	All winter data[b]	0.00[a]	0.01	0.03	0.13	0.27	0.55	107,970
	All summer data[c]	0	0.00[a]	0.00[a]	0.01	0.07	0.92	64,604
		Sea-surface temperature (°C)						*N*
		< − 2.0	[−2.0, −1.0⟩	[−1.0, 0.0⟩	[0.0, 3.0⟩	[3.0, 6.0⟩	≥ 6.0	
Vasilyeva, (1971)	Icing	–	0.04	0.04	0.45	0.45	0.02	871
Current paper	Icing	0.01	0.07	0.09	0.37	0.44	0.03	642
	No-icing	0.01	0.07	0.08	0.45	0.36	0.03	939
	All winter data[b]	0.00[a]	0.04	0.03	0.16	0.50	0.27	105,971
	All summer data[c]	0.00[a]	0.02	0.03	0.13	0.33	0.49	62,763

[a] < 1%.
[b] Defined to be in the period 22 September to 15 May when icing has been observed.
[c] Defined to be in the period 16 May to 21 September when icing has not been observed.

temperature of the icing and no-icing events there is evidence that these values are not significantly different at the 5% level, i.e. $p > 0.05$ (Ch. 3.4 in Chambers et al. (1983)). Although this method is not strictly valid as a formal hypothesis test, it will be applied throughout this study as an indication of whether the medians in the two compared groups are significantly different.

For wave height (H_s), wind speed (V), the angle between the wind and the ship (β), and the total cloud cover (N_N), the confidence intervals of the medians in the icing and no-icing events are spanning different value ranges. Hence, there is evidence that the medians in the two categories for these four parameters are significantly different. In addition to the median values of air temperature, neither the medians of the sea-surface temperature (SST), nor the ship speed (V_s), and nor the relative humidity (R_H) of the two categories are significantly different by comparing the notches in Fig. 3. Although the difference between the median values of the sea-surface temperature of the two categories is small, and the overlap of the notches is indicating non-significance, it is interesting to notice that the icing events occur for higher SSTs than the no-icing events. This was also apparent in Table 2. Intuitively this might seem contradictory since a high sea-surface temperature may inhibit freezing. However, it may indicate that icing occurs in areas with higher sea-surface temperatures due to other factors. The importance of being some distance away from the ice edge in which the lowest sea-surface temperatures arise, and at the same time to have high enough waves for sea-spray icing to take place, is stressed by the verification study of Samuelsen (2018). In general there are lower waves near the ice edge due to fetch limitation when the wind is blowing from the ice. Furthermore, snow showers, particularly intense showers, develop some distance downstream of the ice edge during cold-air outbreaks from the ice. Such solid precipitation may potentially lead to icing in conjunction with sea spray. The fact that icing situations do not have lower relative humidity, and that these events actually have significantly more clouds than the no-icing events, indicates that snow showers may be a contributing factor to icing (Fig. 3). This is

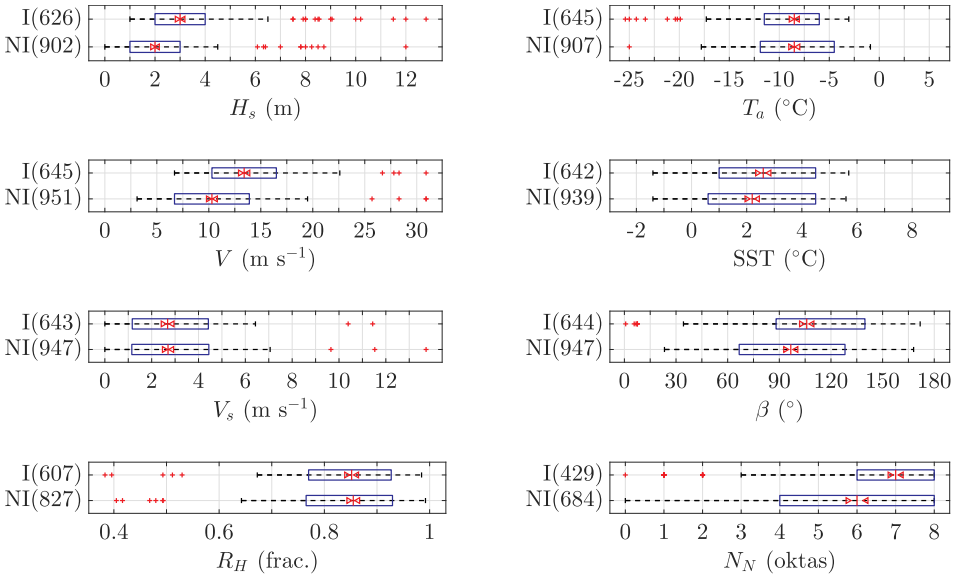

Fig. 3. Box plots of the observed values of important variables in icing events (I) compared to no-icing events (NI). The numbers in brackets indicate the number of valid observations in each category of the particular parameter. The black dashed whiskers represent the 90% confidence interval of a variable in a certain category, outliers are marked with red crosses, and the blue squares represent the interquartile range (IQR) of that variable. The median value of a particular parameter is indicated by a red line, and the triangles around the median are so-called notches illustrating the 95% confidence interval around the medians (median $\pm$ 1.57 $\times$ IQR $\times$ N$^{-0.5}$). Although not equal to a formal hypothesis test, when comparing whether the notches between the icing and no-icing events for a particular variable overlap or not, it provides a strong indication whether the median between the two groups are significantly different at the 5% level (Ch. 3.4 in Chambers et al. (1983)). (For interpretation of the references to colour in this figure legend, the reader is referred to the Web version of this article.)

emphasized when investigating the heat equation (Eq. (1)) since less clouds and lower relative humidity would enhance the evaporative and radiative heat loss leading to a higher probability of ice formation than otherwise, in contrast to what is indicated when comparing the notches of R_H and N_N for the icing and no-icing events in Fig. 3.

The anomaly box plots (Fig. 4) indicate much the same as do the box plots of the absolute values (Fig. 3). However, the air-temperature-anomaly median difference between icing and no-icing is more prominent and significant, and the sea-surface-temperatureanomaly is less prominent and still not significant. This may further underline the fact that the icing events appear in areas and situations more open ocean, i.e. further away from the coastline or ice edge, compared to the areas and situations with no icing. The lower air-temperature anomaly seen in Fig. 4 for the icing compared to the no-icing events, may also be an indirect effect of the wind, i.e. that the icing events occur in situations with stronger cold-air advection. Another interesting signal from the anomaly plots is that approximately 75% of the icing events have higher waves and stronger winds than the climatological values of these parameters. For the no-icing events the median-wave-height anomaly is significantly lower than zero, indicating that the no-icing events occur in conditions with lower waves than the monthly average value inside the latitudinal-longitudinal grid cells of Fig. 2. The median-wind-speed anomaly is on the other hand significantly greater than zero for the no-icing events.

3.3. Cause of icing

It is a well accepted notion that icing due to spray is the most common cause of ship icing (e.g. Zakrzewski (1987) or Zakrzewski and Lozowski (1989)). In fact, following Zakrzewski and Lozowski (1989) this notion is mainly based on statistics from two Russian studies; one study with more than 2,000 observations from several sea areas from around the world collected in the years 1955–1967 (Borisenkov and Panov 1972), and a study with more than 2,000 observations from Arctic sea areas (Barents Sea, Kara Sea, Laptev Sea, East Siberian Sea, and Chukchi Sea) collected in the years 1967–1970 (Kovrova et al., 1969). In addition, Brown and Roebber (1985) collected more than 1,000 observations in Canadian waters from 1970 to 1984 and came to the same conclusions. According to Table 5.1 in Zakrzewski and Lozowski (1989), pure sea spray stands for around 90% of the cause of

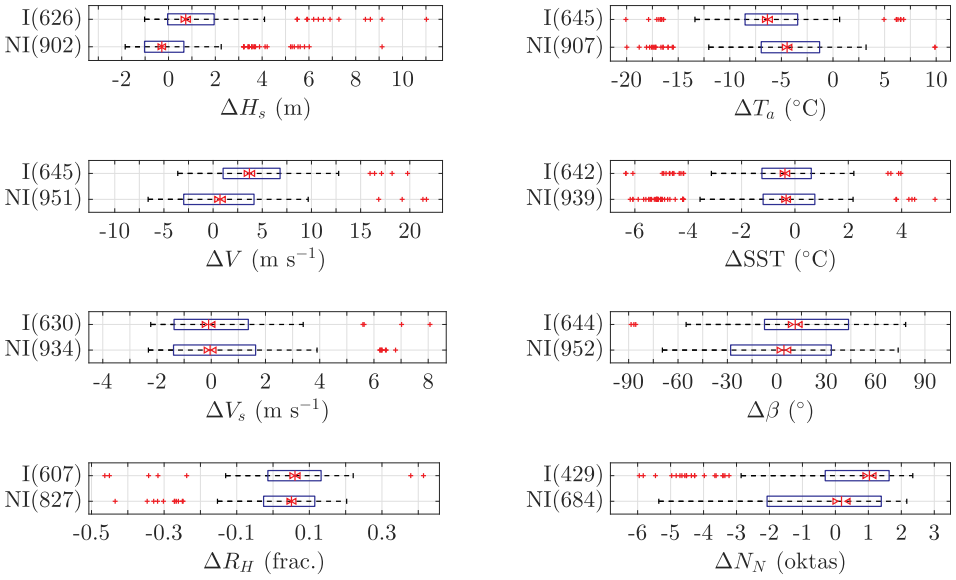

Fig. 4. Box plots of icing (I) and no-icing events (NI) as in Fig. 3, but with anomalies instead of explicit values. The anomalies are calculated by subtracting the mean monthly value from the value of a parameter in a single event. These mean values are derived from all ships operating inside the latitudinal-longitudinal grid boxes visualized in Fig. 2.

icing in most of these studies. However, in Kovrova et al. (1969) only 50% of the icing events stems from pure spray, and 41% of the events from spray in combination with precipitation. Unfortunately it is not clear to which of the atmospheric precipitation sources this statistics refer, i.e. whether the source is freezing rain or snow, since the synop-code parameter cause of icing (I_S) does not include spray in conjunction with snow as a separate option. Consequently, it is therefore possible that the combination of spray and snow may have been recorded under both pure spray icing ($I_S = 1$) or freezing rain and spray in combination ($I_S = 5$). Hence, the 41% may have emerged as result of spray and snow instead of spray and freezing rain as the icing cause in the table of Zakrzewski and Lozowski (1989). A more detailed inspection by Brown and Roebber (1985) determined that only 19% of 960 icing reports from coast guard vessels come from pure spray and 63% from spray and snow combined. A combination of spray and freezing rain appeared in only 0.5% of the events from the east coast of Canada. Icing from pure atmospheric sources ranges in general from 3 to 9% according to Table 5.1 of Zakrzewski and Lozowski (1989).

In the current study the numbers for the different icing causes according to the I_S–parameter are as follows: 539 pure spray-icing events (83.6%), 42 fog-icing events (6.5%), 55 spray and fog icing events (8.5%), two freezing-rain-icing events (0.3%), and seven spray and freezing-rain icing events (1.1%). In the nine events with freezing rain, either alone or in combination with spray, snow is reported in the presented weather code (W_W) in five of the events, including those with pure freezing-rain icing reported. In the remaining four events, one of the events has rain, and the last three events have no recordings of the present weather. In the 42 pure fog-icing events, only eight of the events reported fog in the present weather, while 28 of the events reported snow or snow showers during observation time. Of course fog may still be the major cause of icing in these latter events, but a possibly effect of snow acting together with fog or spray in these events may not be neglected. In any case, from the aforementioned argumentation and statistics, it may be concluded that the idea of summarizing icing data only based on the synop-cause code, is not a sufficient criteria to discriminate the cause of icing. Thus a more detailed inspection of the present weather in all icing events is necessary. Fig. 5 illustrates all present weather codes observed during icing and no-icing events from the current data. In addition, there are 46 icing events with no present weather report, and likewise 129 no-icing events without information about present weather. Solid precipitation, particularly moderate or heavy frontal snow or snow showers ($W_W = 73$–75, and 85–86), seems to be observed more often during icing than no-icing events. Dry weather ($W_W = 00$–09) is observed more often in the no-icing events. For fog observations ($W_W = 41$–49) there is apparently no clear distinction between icing and no-icing events, although, as one might expect, freezing fog ($W_W = 49$) seems to occur in conjunction with icing events more often than in conjunction with no-icing events. Furthermore, from Fig. 5 it seems likely to conclude that freezing rain as a cause of icing may be neglected as a whole in the areas of open water around Northern Norway and the Svalbard archipelago, since there are no icing events in which freezing rain or drizzle is reported in the present weather code ($W_W = 66$–67, and 56–57). However, the single event with non-freezing rain reported together with freezing-rain icing, may have been incorrectly represented as non-freezing.

In order to test the importance of fog and snow more formally, a simple logistic regression model is applied (Table 3). The outcome is then the binary variable icing or no-icing, and different covariates are tested. Firstly, only the present weather code is selected as the covariate. However, since snow showers and evaporation fog occur in situations with strong cold winds over relatively warm waters, parameters like wind speed, wave height, air-temperature, and relative humidity are included in the regression model since these variables may be confounding variables between icing and the present-weather parameters. Based on the findings in Fig. 5 a categorical variable for present weather code is developed; one category equal to frontal snow or snow showers ($W_W = 70$–75, 85 and 86), and one category equal to fog ($W_W = 41$–49). All other types of present weather observations are then assigned to be zero in this variable. From Table 3 it is apparent that the presence of snow in the present weather code increases the probability of icing with a significant odds ratio (OR) of 1.83. In other words there is 83% higher chance of having icing compared to no icing if snow or snow showers are observed based on the data set. For observation of fog the OR is not significant. Furthermore, it is noticeable how the present weather parameter is a confounding variable between icing and relative humidity (R_H). In the model without the present weather information, relative humidity has a weaker and non-significant association to the binary icing variable. However, when the presence of snow and fog is accounted for in the model, the effect of R_H is stronger (β more negative) than if these variables are not accounted for, and with a significant association to icing. Moreover, this fact underlines the importance that the presence of snow showers or frontal snow has on icing. Indeed if the effect of snow on the presence of icing had been negligible, it should not have been affecting the R_H-parameter

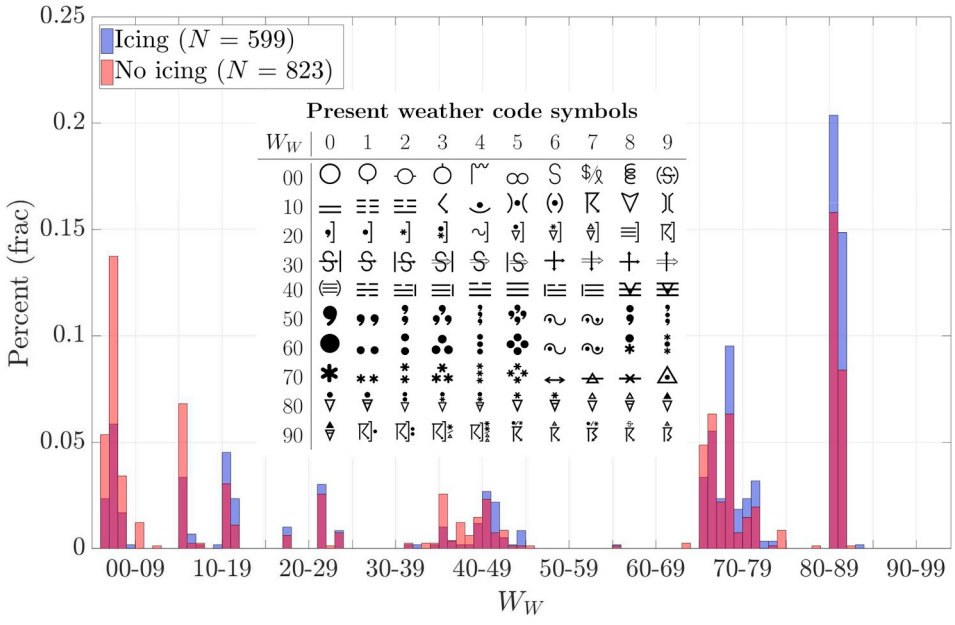

Fig. 5. Histogram of fraction of present weather code observed in icing events (blue shading) and no-icing events (red shading). Purple shadings illustrate fractions covered by both categories. Some weather symbology elements copyright Open Geospatial Consortium are included to illustrate the present weather associated with the code. Details about the present weather code may be found e.g. in WMO (2015). (For interpretation of the references to colour in this figure legend, the reader is referred to the Web version of this article.)

Table 3
Logistic regression model (Eq. (2)) with icing and no-icing as a binary response variable and wind speed (V), wave height (H_s), air temperature (T_a), and relative humidity (R_H) as covariates. The lower panel also includes categorical variables with present weather information (W_W) as covariates[a]. Boldface print indicates that a particular variable with a corresponding coefficient (β_i) and odds ratio (OR_i) has a significant association to the icing/no-icing response variable following Z-value statistics (normal distribution).

Covariate x_i	β_i	OR_i	p-value (Prob.> |Z|)
V	0.06	1.07	1.9×10^{-5}
H_s	0.52	1.69	$< 2.0\times10^{-16}$
T_a	−0.06	0.94	4.1×10^{-6}
R_H[b]	−0.09	0.91	0.105
V	0.06	1.06	1.9×10^{-4}
H_s	0.53	1.70	$< 2.0\times10^{-16}$
T_a	−0.06	0.94	3.3×10^{-5}
R_H[b]	−0.14	0.87	0.020
W_W = snow	61	1.83	3.6×10^{-6}
W_W = fog	0.43	1.54	0.101

[a] Present weather is treated as a categorical variable, separated in these three categories based on the code system of the present weather code of the synop: a category for snow and snow showers for codes equal to 70–75 (frontal snow), 85, and 86 (snow showers), a category for fog for codes equal to 41–49 (fog present at the observing location), and the other W_W observations are assigned to zero. The full present weather code table may be found e.g. in WMO (2015), and is shown with symbols in Fig. 5.

[b] Adjusted to describe the change in a value of 0.1 unit (10%) instead of 1 (100%).

so strongly (Table 3). A possible explanation for the increased risk of spray icing when it is snowing, might relate to the fact that solid precipitation tends to stick with a higher collection efficiency on a wet relative to a dry surface. Snow also provides additional fresh water which will freshen the brine salinity and increase the resulting freezing temperature towards 0 °C. Moreover, the snow dendrites holds a temperature closer to the air temperature, and will often contribute to additional cooling of the brine. Snow dendrites mixed with sea-spray droplets may also contribute to a lower temperature of the incoming spray. Nevertheless, it is difficult to state whether it is the precipitation in itself that is the most contributing factor or if it is the increased turbulence associated with the weather system providing precipitation that is important. Both circumstances may contribute to a higher risk of icing in such weather situations compared to a situation without frontal snow or snow showers.

3.4. Comparing T_{850} in icing and no-icing events

Fig. 6 illustrates the difference in T_{850} between the icing and no-icing events. As opposed to the temperature near the surface, there is a clear indication that the icing events have lower temperatures at 850 hPa than the no-icing events. The median value of T_{850} for the icing events is −19.2 °C, and this is significantly lower than the value of −17.4 °C of the no-icing events. Regarding the threshold suggested by the Japanese and Russian studies in the 1960s and 1970s (Sawada, 1967; Borisenkov and Pchelko, 1975), that icing starts when $T_{850} \leq -18$ °C, around 40% of the icing events in this study have higher temperatures at 850 hPa. However, 95% of the events are lower than −11 °C indicated by the right end of the 90% confidence interval of T_{850}, and 75% below −16 °C, but there are still many no-icing events with temperatures at 850 hPa below these thresholds (Left panel of Fig. 6). When subtracting the monthly mean values of the NORA10 data from the observations for anomaly calculation, a similar pattern is apparent (Right panel of Fig. 6). Almost 75% of the icing events have an anomaly of T_{850} lower than −4 °C, but still more than 50% of the no-icing events have a ΔT_{850} below the same threshold.

4. Large-scale weather situation during icing

4.1. Map composites in icing and no-icing events

As previously stated the 333 icing events that coincide with the junctures of the NORA10 upper-air data are consolidated into 166 different weather situations, and the 486 no-icing events into 183 weather situations. The NORA10 output parameters from all of these events are averaged, and the resulting average mean sea level pressure (MSLP) and temperature at 850 hPa (T_{850}) are plotted in Fig. 7. If numerous icing events had appeared in diverse weather conditions no clear signal would have been perceptible in Fig. 7. However, when comparing the map composites in Fig. 7 a) to Fig. 7 b) it is apparent that there is lower pressure in the Barents Sea and a stronger horizontal pressure gradient in the areas where the icing events occur compared to the situation and areas of no icing. A discernible feature is that the positions of the events in the two categories are quite similar. In addition, there are colder air masses and lower temperatures in 850 hPa further south in the icing-map composite. The green line in Fig. 7 describes the average position of the 40% ice-concentration isoline ($C_I = 0.4$), which may be regarded as a boundary for spray icing (Samuelsen et al., 2017). There are only minor differences between the extension of the ice cover between the two categories. However, in the areas south of Spitsbergen the isoline of the $C_I = 0.4$ is extending somewhat further south in the no-icing relative to the icing events. An ice edge extending further south may potentially lead to lower waves when the wind is blowing from the northeast due to fetch limitations in the areas south and west of the ice edge compared to the same areas in a situation with an ice edge located further north and east. This might be an explanation, together with the weaker pressure gradient and a less cold air mass, for the high concentration of no-icing events in an area around Bjørnøya (74.51 °N, 19.01 °E) with a similar high concentration of icing events.

The anomaly maps are supporting the signatures from the maps with the explicit values. Fig. 8 illustrates how the icing events coincide with negative anomalies in the temperature at 850 hPa (ΔT_{850}), and a more prominent pressure gradient between Greenland and Novaya Zemlya relative to climatology. The no-icing events on the other hand, although many of those are collected in similar weather situations as the icing events, arise clearly in weather situations with an on average less cold air mass and less prominent pressure gradient relative to climatology when compared to the icing-events anomalies.

4.2. CAO_ICE vs. CAO_MTW situations

4.2.1. Separating different mountain-wave situations

In addition to the CAO_ICE situations where the air is blowing from the relatively flat ice cover onto the sea, low air-temperatures, strong winds, and high waves may also prevail when winds are blowing offshore interacting with the topography of the Svalbard archipelago or Northern Norway (Fig. 1). In these situations the air is interacting with the mountains and the fjords which may lead to mountain waves with downslope windstorms and strong gap winds when the air is strongly stratified (Skeie and Grønås, 2000; Samuelsen, 2007). Föhn warming on

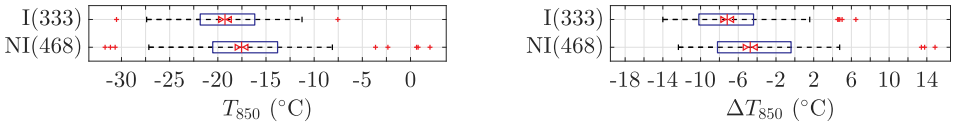

Fig. 6. Box plots of icing (I) and no-icing events (NI) as in Fig. 3, but for T_{850} and ΔT_{850} derived from NORA10.

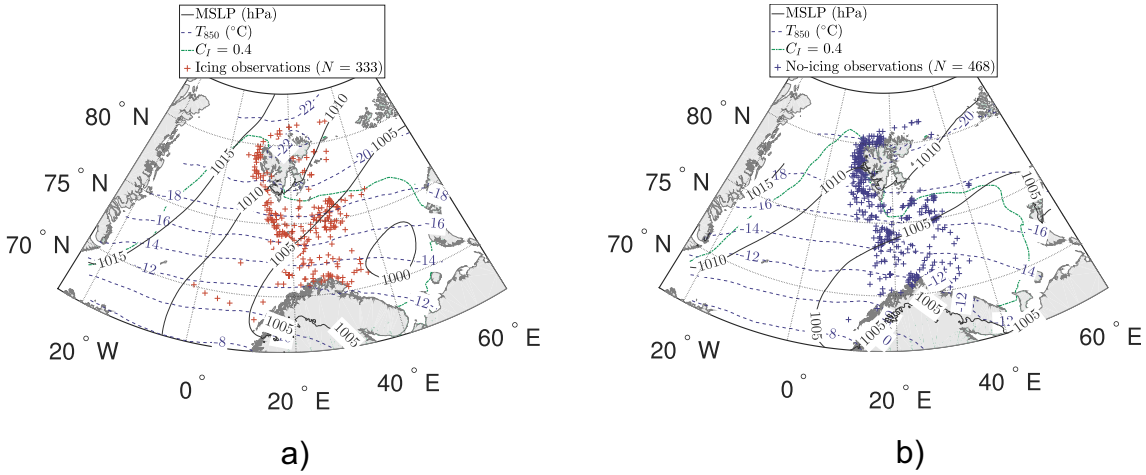

Fig. 7. Map composites in icing and no-icing events. Mean values of the MSLP (black solid lines), T_{850} (blue dashed lines), and the isoline of the C_I = 0.4 (green solid and dashed line) derived from NORA10 of the weather situations in the a) icing events (333 events merged into 166 weather situations), and b) no-icing events (468 icing events merged into 183 weather situations). Line spacing of MSLP is 5 hPa, and the spacing of T_{850} is 2 °C. (For interpretation of the references to colour in this figure legend, the reader is referred to the Web version of this article.)

the lee side of the barrier may enhance stability. In addition, downstream of the barrier this föhn effect will cause attenuation of convection and development of snow showers, and lower the potential for polar-low development. This is in contrast to a situation with cold-air outbreak from the ice. Hence, icing occurring during such mountain-wave conditions are different from those arising in the more terrain-undisturbed northerly wind field when the wind is blowing off the ice. For this reason the CAO_MTW situations are separated from the CAO_ICE situations and both are studied more in detail in the following section.

The CAO_MTW are discriminated from the CAO_ICE situations according to the wind direction and the formation of the topography. The areas offshore of the northern part of Northern Norway are mainly affected by mountain waves when the winds are blowing from around the south (southeast to southwest). Around the Svalbard archipelago these situations mainly occur during easterly flow (northeast to south), either on the west side of Spitsbergen or west side of Nordaustlandet north of Spitsbergen, or during westerly or northerly flow at the east side of Spitsbergen south of Nordaustlandet. These three cold-air outbreak moutain-wave situations are here named and abbreviated as follows: cold-air outbreak mountain-wave situation outside Northern Norway (CAO_MTW NN), cold-air outbreak mountain-wave situation outside Western Spitsbergen (CAO_MTW WS), and cold-air outbreak mountain-wave situation outside Eastern Spitsbergen (CAO_MTW ES).

More details about the selection process of the CAO_MTW events may be found in the Supporting Information (Section S.3). A rough selection using different non-dimensional mountain heights ($\hat{h}$) adopted from Gaberšek and Durran (2004) separating gap flow situations in different flow regimes, also underlines that in more than 95% of both the icing and no-icing events selected based on relatively crude wind-direction and terrain-orientation criteria, mountain waves are most likely present (Section S.3 and Table S.I). Icing and no-icing events not defined according to the CAO_MTW criteria are defined as CAO_ICE. In Fig. 9 the icing events in all of the four categories are plotted with different colours. The CAO_MTW events are also plotted with a wind barb showing their wind speed and direction.

Moreover, Fig. 9 illustrates the average MSLP in the icing situations of the CAO_MTW NN and the CAO_MTW WS. For these two CAO_MTW categories, there are low pressure systems in the Norwegian Sea and higher pressure in the Barents Sea in contrast to the mean weather situation of all icing events (Fig. 7 a)). For the CAO_MTW NN the pressure gradient is oriented west-east with the pressure maximum in the eastern

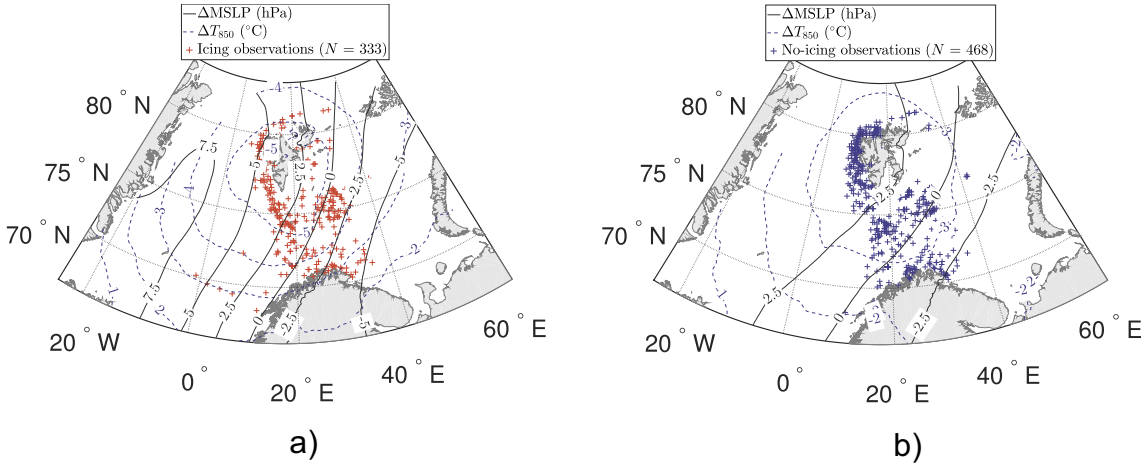

Fig. 8. Map composites of anomalies in icing and no-icing events. As Fig. 7 but with the average values of the anomaly of the mean sea level pressure (ΔMSLP) and the anomaly of the temperature at 850 hPa (ΔT_{850}). Anomalies are calculated by subtracting the mean monthly value of NORA10 from each of the clustered weather situations for a) the icing events, and b) the no-icing events occurring in the same month as the derived monthly value of NORA10. Line spacing of ΔMSLP is 2.5 hPa, and the spacing of ΔT_{850} is 1 °C. Notice that these line spacings are half the size of the line spacing in Fig. 7 in order to see a distinct signal in these maps.

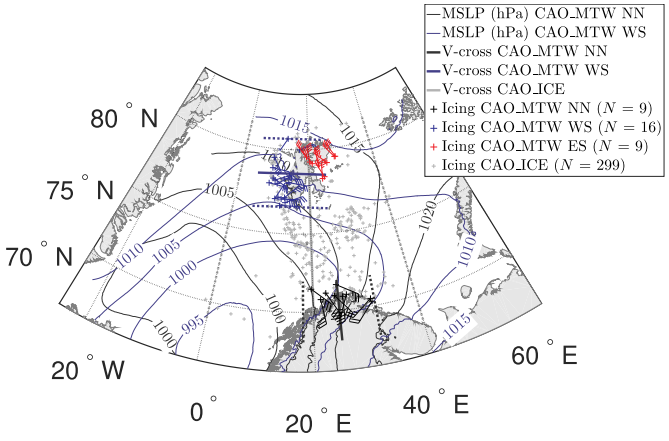

Fig. 9. Overview of observations associated with different weather regimes. Icing events developed during cold-air outbreak mountain-wave situations outside Northern Norway (CAO_MTW NN) are plotted with black crosses, outside Western Spitsbergen (CAO_MTW WS) with blue crosses, outside Eastern Spitsbergen (CAO_MTW ES) with red crosses, and icing events emerged from cold-air outbreak from the ice (CAO_ICE) are plotted with grey crosses. The icing events in mountain wave regimes are also plotted with wind barbs which are describing the wind speed in knots and wind direction of the observed wind on the ship. An overview of the position of the vertical cross-section plots (v-cross) for the CAO_MTW NN, CAO_MTW WS and CAO_ICE regimes applied in Figs. 10–12, are visualized with black, blue, and grey solid and dashed lines, respectively. The solid line is indicating the middle longitude or latitude of the cross section, and the dashed lines are representing the boundary longitudes or latitudes. Average mean sea level pressure (MSLP) are illustrated for the CAO_MTW NN (nine events merged into eight weather situations) and CAO_MTW WS (16 events merged into 14 weather situations) with black and blue solid lines with a contour spacing of 5 hPa. The mean MSLP of the four weather situations (nine events) of the CAO_MTW ES regime, and the mean MSLP of the 147 weather situations (299 events) of the CAO_ICE regime are not illustrated. (For interpretation of the references to colour in this figure legend, the reader is referred to the Web version of this article.)

part of the Barents Sea, while for the CAO_MTW WS the gradient is more north-south oriented with a pressure maximum northeast of Svalbard. The MSLP for the CAO_MTW ES is more similar to the MSLP for all cases, thus the low pressure in the Barents Sea is located further north with a northwesterly flow across Nordaustlandet (not shown). It is also noticeable that there are in general few CAO_MTW situations compared to the CAO_ICE situations, implying that the latter are the clearly dominating scenario for icing encountered on these ships in these areas in the period investigated. For this reason the average MSLP in the CAO_ICE events is quite similar to the average MSLP of all events.

4.2.2. Vertical cross sections

For further comparison between the icing and no-icing events in the CAO_MTW and the CAO_ICE situations, vertical cross-sections are plotted for the CAO_MTW NN, CAO_MTW WS, and the CAO_ICE situations (Figs. 10–12). The cross sections are plotted between 68.0 and 72.0 °N for the CAO_MTW NN (Fig. 10), between 5.0 and 25.0 °E for the CAO_MTW WS (Fig. 11), and between 68.0 and 81.4 °N for the CAO_ICE situations (Fig. 12). The presented cross sections are averages of cross sections calculated every 0.5 ° longitude between 18.0 °E and 32.0 °E for the CAO_MTW NN (Fig. 10), every 0.1 ° latitude between 76.5 °N and 80.5 °N for the CAO_MTW WS (Fig. 11), and every 0.5 ° longitude between 0.0 °E and 40.0 °E for the CAO_ICE (Fig. 12). An overview of the position of the cross sections is provided in Fig. 9. The tangential wind components in the cross sections representing the main flow direction above or below a certain threshold are highlighted with colours. These wind components correspond to the meridional component of the wind (v) for the CAO_MTW NN and the CAO_ICE, and the zonal component of the wind (u) for the CAO_MTW WS. Thus the normal sign convention for the meridional and zonal flow is followed, i.e. a positive sign represents a flow coming from the south or the west, whereas a negative sign represents a northerly or easterly flow. Constant potential temperature lines (isentropes) are applied as streamlines to visualize the ascending or descending motion associated with the flow across the barriers in the CAO_MTW situations. The diabetic effect of condensation or evaporation and other diabatic heating effects on the air flow is then neglected. Differences between the icing and no-icing events are also illustrated in separate plots (Fig. 10 c), 11 c), and 12 c)).

Several interesting patterns are manifested in these cross sections. In the CAO_MTW NN there is a marked southerly jet from around 925 hPa

(a)

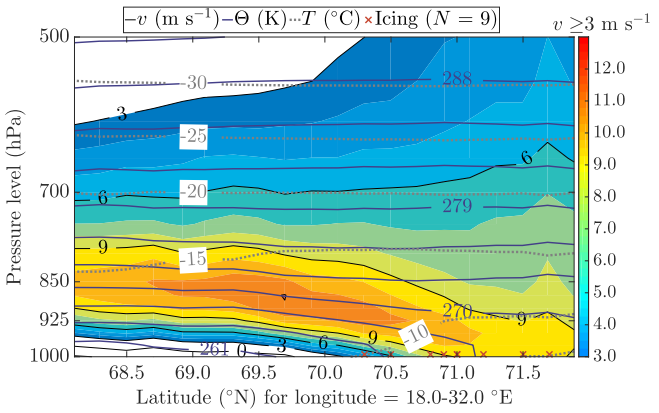

(b)

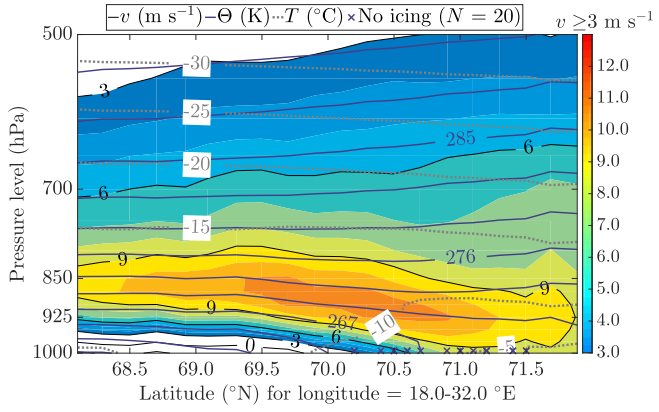

(c)

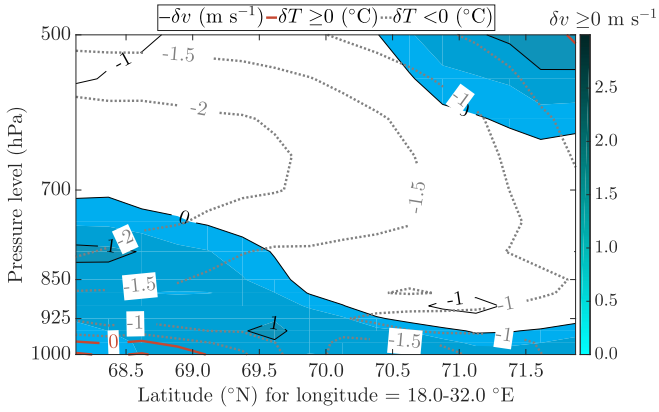

(caption on next page)

Fig. 10. Vertical cross sections for the CAO_MTW NN regime. Averages of cross sections calculated every 0.5 ˚ longitude between 18.0 ˚E and 32.0 ˚E (Fig. 9) are presented for a) the icing events (eight weather situations), b) the no-icing events (13 weather situations), and c) the difference between the icing and the no-icing events. The cross sections are derived from 40 model levels interpolated to pressure levels, and the y-axes are plotted on a logarithmic scale. The meridional component (v) is tangential to the cross section and is plotted with black solid lines with a line spacing of 3 m s^{-1} in a) and b), and in c) the meridional component difference ($\delta v = v_{\text{icing}} - v_{\text{noicing}}$) is plotted with a line spacing of 1 m s^{-1}. In a) and b) the meridional winds above 3 m s^{-1} are plotted with colours. In c) positive wind component differences are plotted with colours, i.e. when there are stronger southerly winds in the icing compared to the no-icing events. Isentropes (Θ–lines) are plotted with a solid blue colour with 3 K line spacing in a) and b). Air temperature is plotted as grey dotted lines with a line spacing of 5 ˚C in a) and b). In c) the air-temperature difference ($\delta T = T_{\text{icing}} - T_{\text{noicing}}$) greater or equal to zero is plotted as red solid lines with a line spacing of 1 ˚C, and δT<0 ˚C is plotted with grey dotted lines with a line spacing of 0.5 ˚C. The latitudinal position of the icing and no-icing events are plotted with a) red crosses and b) blue crosses near the 1000 hPa level in a) and b). (For interpretation of the references to colour in this figure legend, the reader is referred to the Web version of this article.)

to 850 hPa upstream of the coastline located around 70–71 ˚N (Fig. 10). Downstream of the coastline the jet is located at lower levels, and the strongest winds are extending further down in the icing compared to the no-cing events. The air is also colder in the icing compared to the no-icing events with the largest differences between the icing and the no-icing events from 850 hPa to 500 hPa upstream, and around 1000 hPa in the areas of the observations downstream. The jet in itself is associated with lee-side acceleration due to mountain-wave activity over the mountain areas of Northern Norway in a statically stable environment, and this is visualized by the fact that the isentropes extending up to around 925 to 850 hPa upstream are pushed downwards and intersecting 1000 hPa in the areas downstream. Due to the adiabatic heating during the descent, the air has a higher temperature downstream than it otherwise would have had. However, in the icing events the air masses are still cold enough for icing to be encountered. This kind of phenomenon is often classified as bora (Jurčec, 1980). Indeed the terrain of Northern Norway is a combination of fjords and mountains, and gap-flow acceleration through the fjords also arises. However, it is not uncommon that gap flows occur in conjunction with mountain waves with downslope windstorms in general (Gaberšek and Durran, 2004) or more particularly in Northern Norway (Samuelsen, 2007). In fact, more than 60% of the icing and no-icing events in CAO_MTW NN are in the so-called mountain-wave regime applied in Gaberšek and Durran (2004), and mountain waves are probably involved also in the other regimes (Table S.I). Hence, based on this argumentation and the vertical cross sections, it is reasonable to state that the icing events in the CAO_MTW NN situations are encountered in stronger and colder bora-like events over Northern Scandinavia compared to the no-icing events.

For the easterly flow over the Spitsbergen island in the Svalbard archipelago in the CAO_MTW WS case, the situation is somewhat different (Fig. 11). First and foremost the overall air masses are colder than in the CAO_MTW NN case. The upstream conditions around 850 hPa between the icing and no-icing events are here quite similar, and the easterly flow is in fact stronger in the no-icing events compared to the icing events at this level (Fig. 11 c)). Downstream of the barrier, mainly west of 15 ˚E, there are mostly stronger easterly winds in the icing compared to the no-icing events from 850 hPa and down to 1000 hPa. The wind speed and not only the easterly component of the wind is also in general stronger in the icing compared to the no-icing events at these low levels for the CAO_MTW WS scenario (not shown). On the other hand, the mean temperatures are up to 2 ˚C higher below 925 hPa in the icing compared to the no-icing events in the areas of the ship observations. These somewhat higher temperatures apparent in the icing events are probably encountered due to the fact that the air is

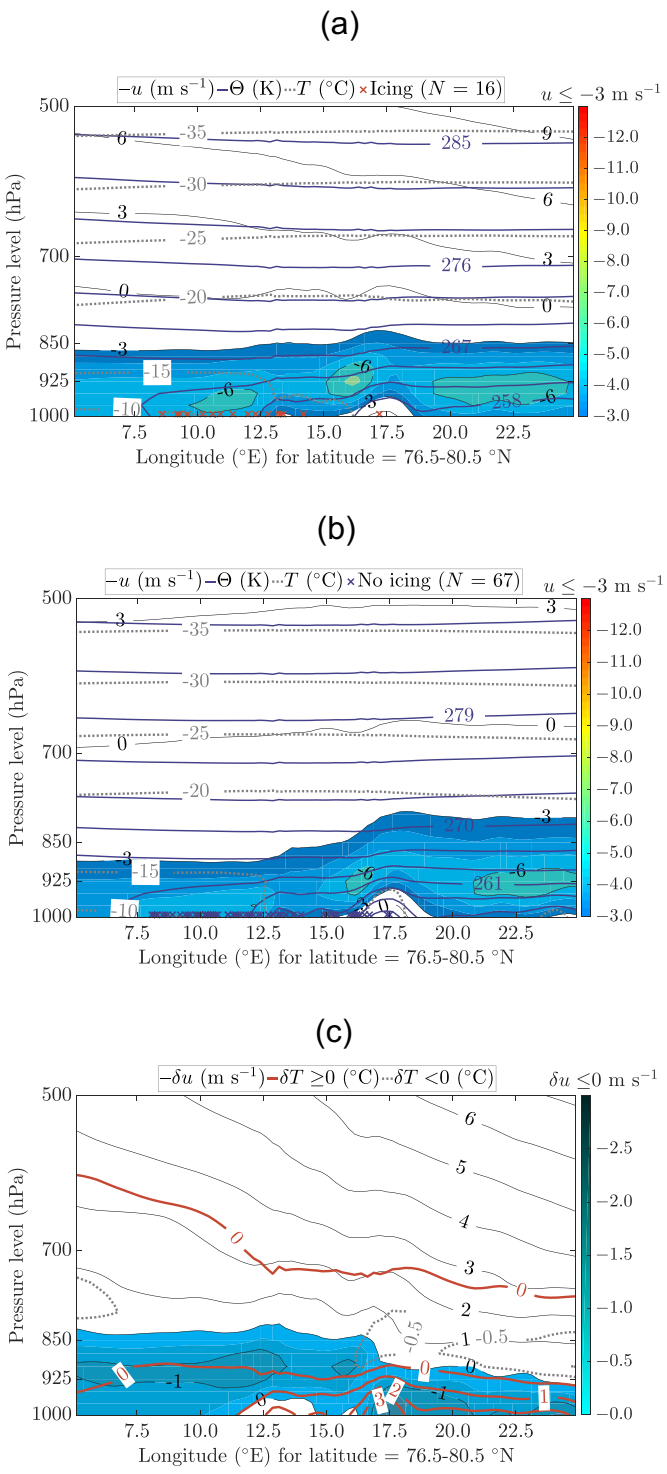

Fig. 11. As Fig. 10, but for the average value of the parameters in the CAO_MTW WS regime. Averages of cross sections calculated every 0.1 ˚ latitude between 76.5 ˚N and 80.5 ˚N (Fig. 9) are presented for a) the icing events (14 weather situations), b) the no-icing events (34 weather situations), and c) the difference between the icing and the no-icing events. The zonal component (u) is here tangential to the cross section, and is therefore plotted with black solid lines instead of v. Zonal winds below −3 m s^{-1} are plotted with colours in a) and b). In c) the differences between the zonal components of the weather situations in the icing and the no-icing events ($\delta u = u_{\text{icing}} - u_{\text{noicing}}$) are plotted with black solid lines, and in colours for negative zonal-wind-component differences, i.e. there are stronger easterly winds in the icing compared to the no-icing events. The longitudinal position of the icing and no-icing events are plotted with a) red crosses and b) blue crosses near the 1000 hPa level in a) and b). (For interpretation of the references to colour in this figure legend, the reader is referred to the Web version of this article.)

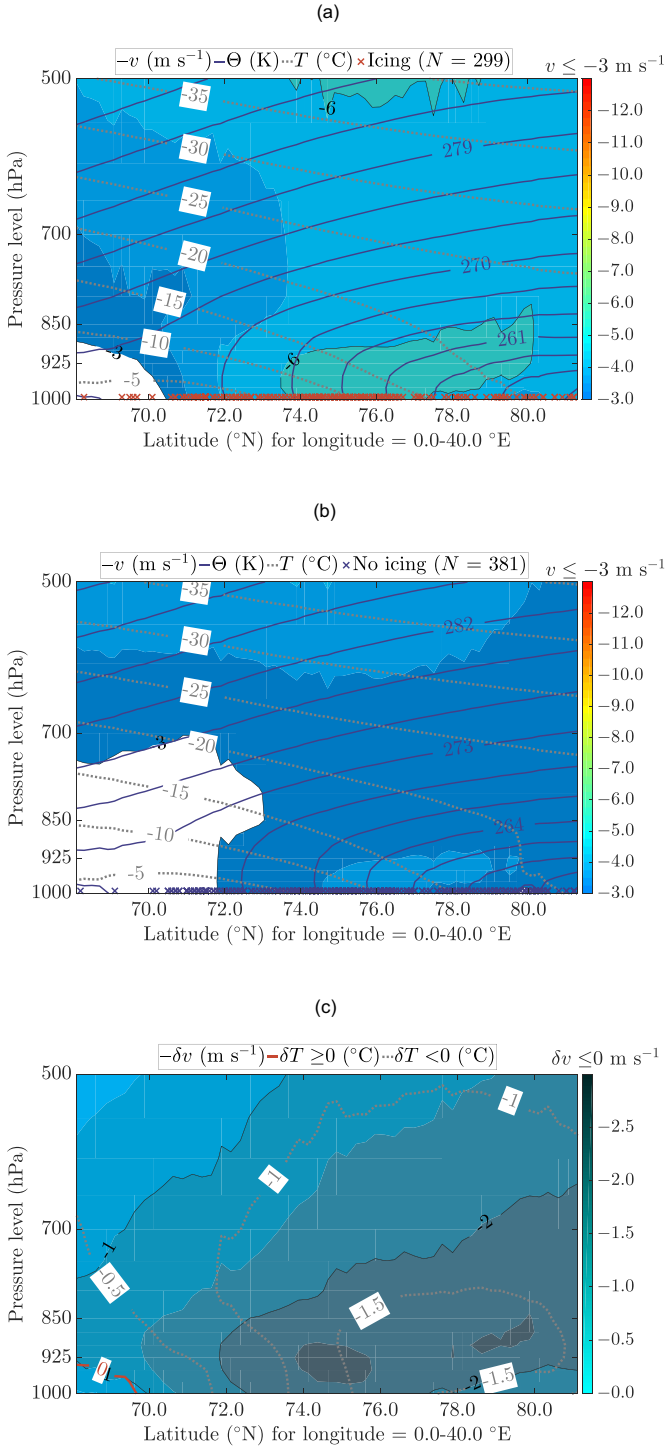

Fig. 12. As Fig. 10 but for the average value of the parameters in the CAO_ICE regime. Averages of cross sections calculated every 0.5 ° longitude between 0.0 °E and 40.0 °E (Fig. 9) are presented for for a) the icing events (147 weather situations), b) the no-icing events (163 weather situations), and c) the difference between the icing and the no-icing events. The meridional component is here plotted in colours for meridional winds below $-3\,\mathrm{m\,s^{-1}}$ in a) and b), and in c) in colours for negative meridional-wind-component differences, i.e. there are stronger northerly winds in the icing compared to the no-icing events. (For interpretation of the references to colour in this figure legend, the reader is referred to the Web version of this article.)

adiabatically warmed but still cold enough for icing to arise, and consequently wind and waves are more important parameters in determining whether icing will occur or not in these situations.

Regarding the generation of waves there is in this area sea ice in the fjords in contrast to the fjords of Northern Norway where little sea ice is encountered. There are also indications by investigating the isoline of the 0.4 ice concentration in Fig. 7 that the ice edge is located further west in the no-icing relative to the icing situations. This fact is also apparent when studying the horizontal map composite of the CAO_MTW WS icing and no-icing scenario isolated from each other (not shown). Due to the relatively crude resolution of the NORA10, it is not possible to determine accurately the sea-ice cover inside the fjords, but it is reasonable to assume that there might be some lower fetch during easterly flow in the no-icing compared to the icing events for the CAO_MTW WS. A shorter fetch length due to the presence of sea ice will generate lower waves for the same wind speed. The median of the observed wave heights is also significantly higher in the icing compared to the no-icing events, although the median of the observed wind speeds is not significantly different (Supporting information Fig. S.2).

Another interesting aspect in the CAO_MTW WS situation, is the presence of a marked reversed flow aloft (westerly). In mountain wave theory (e.g. Durran (1990); Markowski and Richardson (2011)) a presence of a mean-state critical layer, i.e. where the tangential wind changes sign, might induce wave breaking aloft which provides presence of a downslope windstorm at the lee side of the barrier. A critical layer located closer to the mountain top might induce more energy reflection and stronger winds downslope of the barrier than a critical layer located at higher levels. In the icing events the height of the critical layer is lower than in the no-icing events, and there is also a stronger westerly flow aloft. Based on this fact the probability of wave breaking is higher in the icing compared to the no-icing events, and consequently this might be a feasible reason for the stronger easterly flow present downstream in the icing events. However, it is also possible that wave breaking occurs in both cases, but that the strength of the downslope windstorm and the gap flows are stronger in the icing events. Although a critical layer is not present in the CAO_MTW NN, there is a stronger negative wind shear in the icing compared to the no-icing events (Fig. 10). Such a stronger reversed shear might also enhance a downslope windstorm and explain the stronger winds in the NORA10 of the icing compared to the no-icing events of the CAO_MTW NN (Markowski and Richardson, 2011).

The CAO_ICE situations on the other hand reveal a distinctly different flow pattern (Fig. 12). Unstable air masses are developed in a deep layer when the cold air from the ice is moving over the relatively warm ocean. The areas over pure open ocean, especially south of around 76 °N south of Spitsbergen, have clearly more vertically tilting isentropes indicating weak stratification with possibly instabilities and convection. In general there is a more constant-with-height average flow from the same direction in these situations in contrast to the CAO_MTW situations. As indicated by the difference plot (Fig. 12 c)), the average northerly wind is stronger, and the temperature is lower in icing relative to no-icing events for almost all latitudes all the way up to 500 hPa above the areas of the ship observations. However, at the lowest latitudes (around 68–72 °N) there is a somewhat less negative or positive temperature difference from around 925 hPa and below. On the other hand, at around 850 hPa to 700 hPa the temperature difference between icing and no icing is more negative also at these latitudes. This underlines why T_{850} might be a better indicator of icing than just the temperature at lower levels in such situations.

4.2.3. *Vertical profiles*

A further illustration of the difference in the stratification between the CAO_ICE and the CAO_MTW events as a whole is also shown in Fig. 13. The temperature profiles in this figure visualize how on average the lowest layers of the NORA10 atmosphere above each of the observed icing and no-icing events position in the CAO_MTW scenario are clearly more statically stable than these layers in the CAO_ICE scenario. Notice that the profiles are calculated without considering autocorrelation related to similar weather conditions as in the vertical cross

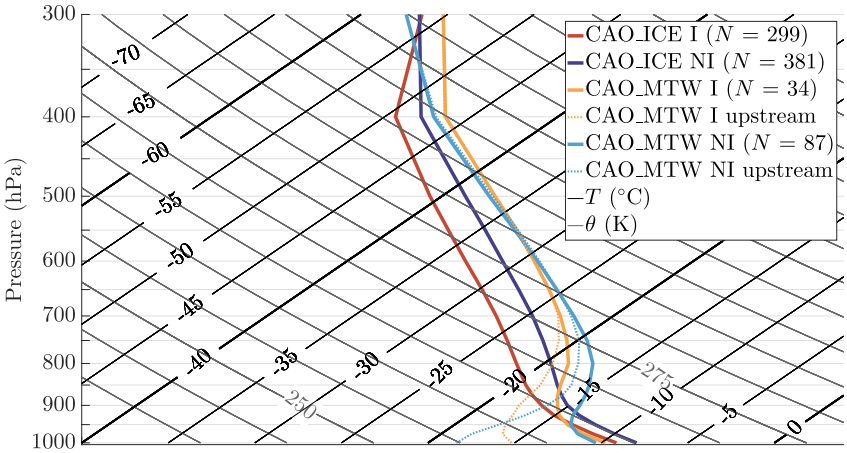

Fig. 13. Mean vertical temperature profiles above the position of all icing and no-icing events in the CAO_ICE and the CAO_MTW regimes. For the CAO_MTW regime the upstream values are also plotted. For CAO_MTW NN a latitudinal position of 68.5 °N and the observed longitude of the ships are selected as the upstream positions of the data, for the CAO_MTW WS a longitudinal position of 22.5 °E and the observed latitude of the ships are selected, and for the CAO_MTW ES the position of 80.5 °N 20.0 °E is applied.

sections plots. The larger T_{850}–difference between the icing and the no-icing events for all scenarios relative to the temperature differences between these two categories in the layers near the surface are also clearly shown by this plot. Another signature of the profiles is that for the CAO_MTW scenario there is in general more turbulent mixing for the icing compared to the no-icing events. This is probably a result of the stronger winds in the icing compared to the no-icing events as is apparent in Figs. 10 and 11. Fig. 13 also indicates that it is on average a smaller difference between the T_{850} of the CAO_ICE scenario and the CAO_MTW upstream scenario, than the difference between the CAO_ICE and the CAO_MTW above the ship locations. Upstream positions (Fig. 13) for the CAO_MTW NN and the CAO_MTW WS regimes are selected based on values in the plotted cross sections (Figs. 10 and 11), and for the CAO_MTW ES regime a representative position north of Nordaustlandet is selected as a fixed upstream position for all of these nine events. The application of values from some upstream positions for the CAO_MTW scenario instead of the values above the ship positions is further elaborated in Section 5.2.

4.2.4. Vertical cross sections with humidity

In order to investigate differences in humidity between the icing and no-icing events in the three proposed weather situations (CAO_ICE, CAO_MTW NN, and CAO_MTW WS), vertical cross sections are also plotted showing the difference in specific and relative humidity between icing and no icing (Fig. 14). Relative humidity is here derived by applying the average value of the temperature and specific humidity in the cross sections. It is decided to not present this parameter as an average of R_H calculated directly for each weather situation, since the R_H-parameter is right-skewed towards 1.

For the CAO_MTW NN (Fig. 14 a)) it is apparent that the icing events are encountered in situations with less relative humidity upstream and somewhat higher relative humidity downstream at the lowest levels. This increased relative humidity downstream may be a result of the difference in temperature between the icing and no-icing events. For a constant flux of vapour from the relatively warm and humid surface of the ocean, the relative humidity would increase the most in the situations with the lowest temperatures, and it is observed that the temperatures are the lowest in the icing compared to the no-icing events for the CAO_MTW NN (Fig. 10). However, a colder and drier air mass advected with a stronger and more turbulent wind over a relatively warm and humid surface, also implies increased sensible and latent heat fluxes from the sea surface compared to an air mass with less cold, less dry, and weaker winds with less turbulence advected over an ocean surface with similar temperatures. Thus, brine water on a ship may also be subjected to additional convective and evaporative cooling in such conditions (Eq. (1)). Increased evaporation due to the drying out of air in downslope flows has also been suggested to be of relevance in wet-snow-icing events in Iceland (Olafsson et al., 2002). An increase in the flux of vapour due to an increased latent heat flux from the sea will also increase the humidity and hence the relative humidity. This is consistent with the difference in specific humidity decreasing downstream when comparing icing and no-icing situations (Fig. 14 a)). In fact, the specific humidity is in general the lowest in the icing events in almost the entire cross section. The drier atmosphere at several layers would enhance the longwave radiative cooling effect in the icing compared to the no-icing events, and this may be an additional reason why the former events encounter icing compared to the latter ones. On the other hand, the effect of longwave-radiative cooling is in general low compared to the cooling of the brine water on the ship from the convective/sensible and evaporative/latent heat fluxes of the atmosphere (Samuelsen et al., 2017). Hence, the cooling from the Q_r-term (Eq. (1)) may still be the final effect pushing the situation over the threshold from no icing to icing.

The CAO_MTW WS exhibits quite different characteristics compared to those at the CAO_MTW NN when it comes to humidity. In Fig. 14 b) there is pronounced higher relative humidity at most levels in the icing compared to the no-icing events. The maximum relative humidity is encountered in an area around 850 hPa both upstream and downstream of the barrier. This is probably an indication that the icing in these situations are associated with more clouds and precipitation due to increased frontal activity. This might also stem from an increased orographic intensification of clouds with or without precipitation over the Spitsbergen island in the icing compared to the no-icing events due to warmer and more humid air masses in the former events. 38% of the 16 icing events report frontal precipitation in the present weather code, and for the no-icing events the amount is 30% out of a total number of 67 events. There are only a few reports of showers in both categories. In addition, there might also be situations where the precipitation is only manifested over the mountains, and not reaching the location downstream where the ships are present due to the drying effect from the adiabatic descent of the cross-barrier flow. This is indicated by smaller differences in both relative and specific humidity at the lowest levels downstream of the barrier. Although the precipitation in itself might intensify the icing, the presence of a front might also contribute to the increased easterly wind speed downstream of the barrier (Fig. 11).

In the CAO_ICE situations the differences in relative humidity between the two categories icing and no-icing are much smaller. However, there is still some indication that there is higher relative humidity from around 925 hPa up to around 700 hPa in the areas south of around 77 °N in the icing compared to the no-icing events. This may follow up on the argumentation of Section 3.3 that the presence of showers may be important for icing to be encountered in the CAO_ICE situations. In addition to more precipitation, more showers or more intense showers, may also provide stronger wind gusts and more turbulence. More turbulence increases the convective (sensible) and evaporative (latent) heat fluxes from the salty water on the ship to the

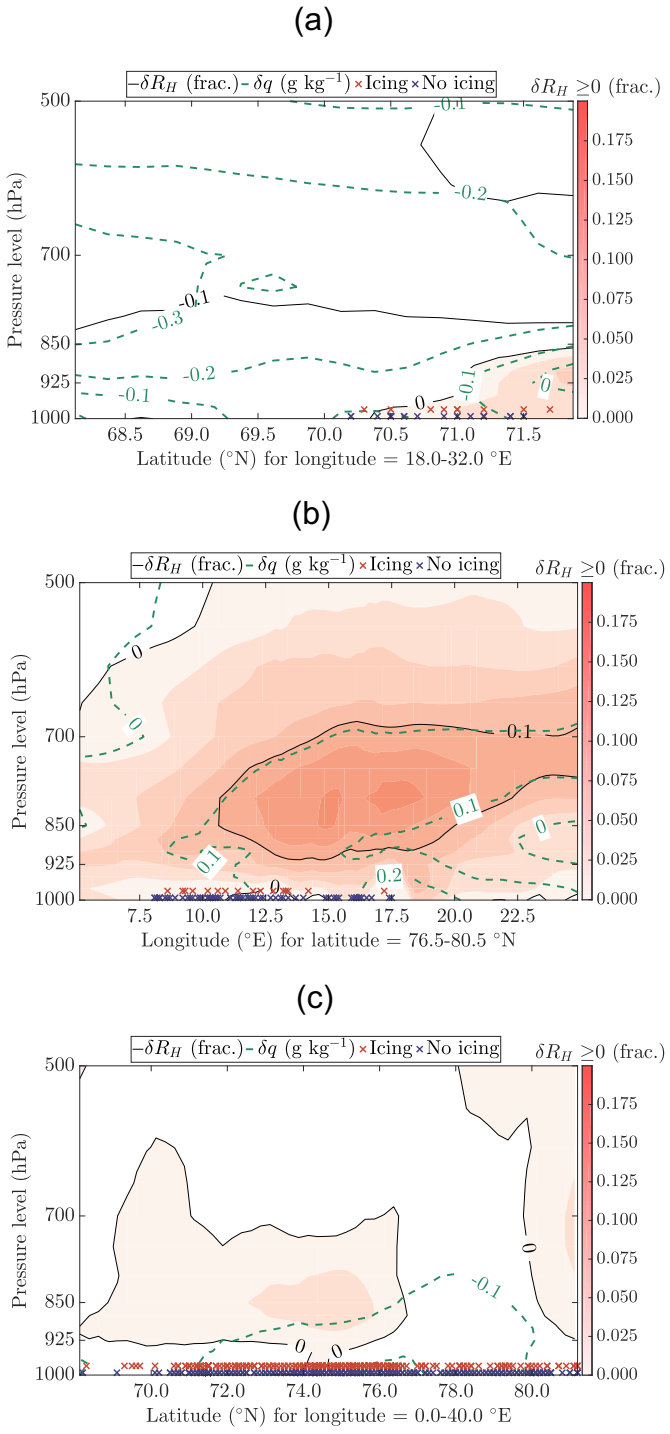

Fig. 14. Average vertical cross sections as in Figs. 10, 11, and 12 for specific and relative humidity differences. The difference between the icing and the no-icing events is plotted for a) the CAO_MTW NN regime, b) the CAO_MTW WS regime, and c) the CAO_ICE regime. Specific-humidity difference ($\delta q = q_{\text{icing}} - q_{\text{noicing}}$) is plotted as dashed green lines with a line spacing of 0.1 g kg^{-1}. Relative humidity is derived by applying the average specific humidity and temperature values from the cross sections. The relative-humidity difference ($\delta R_H = R_{H-\text{icing}} - R_{H-\text{noicing}}$) is plotted as black solid lines with a line spacing of 0.1 (10%). Positive values of δR_H are plotted with colour shading, i.e. there is higher relative humidity in the icing compared to the no-icing events. The a) and c) latitudinal or b) longitudinal positions of the icing and no-icing events are plotted with red and blue crosses, respectively, near the 1000 hPa level. (For interpretation of the references to colour in this figure legend, the reader is referred to the Web version of this article.)

atmosphere hereby enhancing the cooling of the brine and increasing the risk of icing (Section 2.1). The aspect of wind gusts and turbulence may also play a role in explaining why the icing events are encountered in CAO_MTW situations with stronger downslope windstorms which potentially have stronger turbulence compared to the no-icing events in such situations.

5. Simple model for icing probability

5.1. Verification of upper-air and surface parameters in NORA10

For prediction of icing longer than the nowcasting period, the accuracy of the variables derived from numerical weather-prediction models is essential. As mentioned in the introduction, the skill of the forecast of variables from numerical weather-prediction models degrades with forecast lead time, and the skill degrades faster for the variables near the surface in the boundary layer, than for those at higher levels. For the NORA10 it is also interesting to compare the quality of the surface and upper-air variables relative to observations. As seen in Table 4, T_{850} has smaller errors relative to observations than both T_{1000} using data collected from three radiosonde stations north of 67 °N, and the T_{2m} compared to the observed temperature (T_a) of the ships. It is noticeable that there is a clear positive mean error (BIAS) of T_{2m} which is the highest in the icing events compared to those events where both icing and no-icing are merged together. Likewise there is a clear and more negative BIAS of V_{10m} in the icing events compared to the combined events. It is also apparent that both wind variables (V_{850} and V_{1000}) at the radiosonde stations have smaller BIAS in absolute value than V_{10m}, but the mean absolute error (MAE) is still quite high, i.e. around 3 m s^{-1}.

5.2. Logistic regression model with upper-air parameters

The fact that there are smaller errors in the representation of the variables at higher levels of a model is not only apparent from the verification of a reanalysis data set, but also when comparing errors between T_{2m} and T_{850} for predictions of a couple of days ahead in time (e.g. underlined in Haiden et al. (2016) by comparing the RMS error in T_{850} in Fig. 7 and T_{2m} in the same paper for lead times of 60–72 h in the ECMWF model). For these reasons it is interesting to follow the pathway of the Japanese and the Russian studies in the 1960s and 1970s which applies parameters at 850 hPa to forecast icing (Sawada (1967); Sawada (1968); Vasilyeva, (1971); Borisenkov and Pchelko

Table 4
Mean error (BIAS) and mean absolute error (MAE) of NORA10 surface variables and NORA10 upper-air variables.

Variable[a]	BIAS		MAE		*N*	
	Icing	Both	Icing	Both	Icing	Both
T_{2m} (°C)	1.5	1.2	1.7	1.7	168	379
V_{10m} (m s^{-1})	−2.5	−1.9	3.1	3.0	168	388
MSLP (hPa)	0.7	0.6	1.5	1.3	168	387
H_s (m)	−0.2	−0.1	1.0	0.9	155	343
T_{850} (°C)	−0.4		1.3		887	
V_{850} (m s^{-1})	−0.3		2.6		885	
T_{1000} (°C)	2.2		2.5		613	
V_{1000} (m s^{-1})	0.3		2.5		606	

[a] The variables of the upper panel are collected from the ships, while the variables of the lower panel are collected from the radiosonde stations at Bjørnøya (74.51 °N, 19.01 °E), Jan Mayen (70.93 °N, 8.65 °W), and Bodø (67.25 °N, 14.40 °E) (Fig. 1). The ship observations from both the icing and no-icing events, and the radiosonde data are collected from the same junctures. Since the radiosonde data are only available at 0000 and 1200 UTC only the ship observations which are collected at these times are applied in the table.

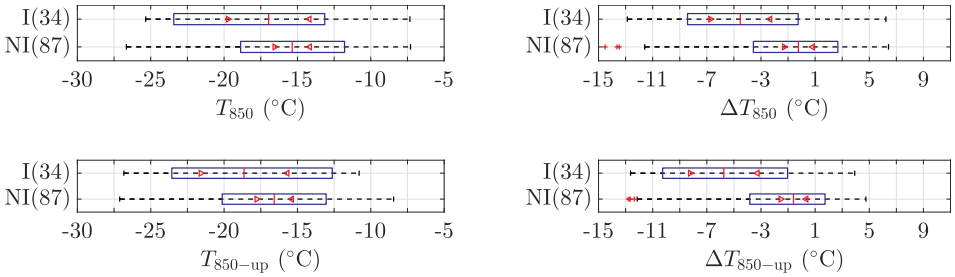

Fig. 15. Box plots of icing (I) and no-icing events (NI) as in Fig. 6, but for the three CAO_MTW situations merged. The upper panels illustrate the parameters collected from a position just above the ship, and the lower panels when the parameters are collected from a position upstream of the barrier (see Fig. 13 for details about the upstream positions applied).

(1975)). Moreover, a low T_{850} over relatively warm water, is an indirect signal of convection, static instability, and showers, which according to the aforementioned results increase the risk of icing. The paper of Sawada (1967) also indicates observations of solid precipitation in connection with icing. However, as illustrated by the Fig. 6 and the Fig. 7 a criteria of $T_{850} \leq -18$ °C would exclude around 45% of the icing events in total in the current study, and around 55% of the events when considering the warmer and more stratified conditions of the CAO_MTW isolated (Upper panel of Fig. 15). Based on the information from the vertical cross sections and the vertical profiles in the CAO_MTW situations, the temperature at 850 hPa upstream of the barrier is applied instead of a position right above the ship location in the model development. In particularly for the CAO_MTW NN the temperature differences between the icing and no-icing events were notably more negative upstream at this level (Fig. 10 c)). For the CAO_MTW situations as a whole there is also a marked change in the difference between the T_{850}–values of the two categories icing and no icing when applying the upstream values compared to the values at a position above the ship location (Figs. 13 and 15). However, only the median values of the anomalies of T_{850} (ΔT_{850}) for the icing and no-icing events are significantly different from each other also for the upstream conditions. According to Fig. 8 it is also apparent that most icing events arise in areas and conditions with an on average lower temperature anomaly in 850 hPa (ΔT_{850}) compared to those of no icing.

Logistic regression models are derived by dichotomizing the predictors of the parameters of T_{850} and ΔT_{850} in a criterion of being either above or below a certain threshold. When applying ΔT_{850} as a predictor alone, significant covariates ($p< 0.05$), and the lowest Akaike information criterion (AIC), i.e. a measure for the relative goodness of fit (Vittinghoff et al., 2011), are obtained when ΔT_{850} is lower or equal to a value of about -4 or -5 °C. From the information in Figs. 6 and 8 these values seem reasonable to apply as thresholds for icing, specifically for the CAO_ICE situations and the upstream value of the CAO_MTW situations. In order to make sure that the air masses are cold enough for icing to be encountered, it is necessary to consider the actual value of temperature as well. Thus, in addition to applying a threshold of $\Delta T_{850} \leq -4.0$ °C, logistic regression models with different thresholds for T_{850} are added to the same model. From the training data set it is found that the best fit is achieved when the $T_{850} \leq -11$ °C or $T_{850} \leq -15$ °C combined with the selected threshold of ΔT_{850}. A criterion of $T_{850} \leq -15$ °C is applied in order to ensure that the surface temperature is negative when applying such upper-air temperatures in well-mixed conditions. This will for instance be the case if the vertical temperature gradient is set to -1 °C (100 m)$^{-1}$ (well-mixed conditions), and the Z_{850} is not more than 1500 m. The maximum height of Z_{850} in the icing events is 1492 m derived from NORA10.

The advantage of applying the ΔT_{850}–variable is that it includes some information about advection of air masses from colder areas in contrast to the T_{850}–variable alone. This is specifically the case over open ocean where the temperature would rise to a higher value than otherwise if the advection stops due to convection and mixing from the relatively warm ocean. If including the wind speed at 850 hPa as well, some information is obtained about how fast the air is advected from the cold land or sea ice to the icing location at this altitude. A stronger wind at this level would impede the warming effect from below. When applying the aforementioned criteria of ΔT_{850} and T_{850}, the best model fit is obtained by applying a value of around 8 m s^{-1} in V_{850} as a lower boundary for icing. As for the other two parameters the upstream values are applied for the CAO_MTW situations.

Table 5 summarizes the verification scores of some of the models evaluated. In the upper panel of this table the model of the Japanese and Russian studies, which applies a single criteria of $T_{850} \leq -18$ °C, is compared to a model including criteria for both ΔT_{850} and T_{850}. Although this latter model has more overestimations than the single-parameter model, according to the bias ratio, all the other scores have higher values indicating better performance in this model compared to the single-parameter one. If including the wind speed at 850 hPa with the selected threshold of 8 m s^{-1} as an additional dichotomized parameter in the logistic regression model, the performance of the model is enhanced compared to the other two models measured by the verification scores in the control data set (Table 5). The bias ratio is indeed equal to 1.0 in this model, and the percentage of hits and correct negatives are almost 70%. It is compelling to compare the scores of these upper-air parameters with the scores calculated by models using more commonly-applied criteria derived from some surface parameters (lower panel of Table 5). Firstly, the application of the isoline of either the zero temperature or the freezing temperature of sea water of around -2 °C, have poor performances with a PC less than 50% meaning that there in fact are more misses and false alarms than correct icing or no-icing predictions.

Some studies apply combinations of temperature and wind speed with or without a criterion for sea-surface temperature as an indication of icing (Mertins, 1968; DeAngelis, 1974; Borisenkov and Pchelko, 1975). Even the ISO 19906: An International Standard for Arctic Offshore structures (Section A.6.3.5.3 in International Organization for Standardization (ISO, 2010) applies such criteria for offshore structures although these are developed based on the icing risk of ships. However, instead of testing and listing up all criteria between these surface parameters and icing that exist in the literature, the commonly-applied criterion of the nomogram of Mertins (1968) is applied and tested along with the other models ($T_{2m} \leq -2$ °C, $V_{10m} \geq 10.8$ m s^{-1}, SST ≤ 8 °C). The

Table 5
Verification scores[a] of 2 × 2 contingency tables for predicted and observed events for different models tested on the control data set (N = 261).

Model	PC	BIASr	ETS	HSS	PSS
$T_{850} \leq -18$ °C	0.55	1.31	0.05	0.10	0.11
$\Delta T_{850} \leq -4.0$ °C, $T_{850} \leq -15$ °C	0.59	1.39	0.11	0.19	0.21
$\Delta T_{850} \leq -4.0$ °C, $T_{850} \leq -15$ °C, $V_{850} \geq 8$ m s^{-1}	0.67	1.00	0.17	0.29	0.29
$T_{2m} \leq 0$ °C	0.42	2.53	0.02	0.05	0.06
$T_{2m} \leq -2$ °C	0.45	2.31	0.04	0.07	0.09
$T_{2m} \leq -2$ °C, $V_{10m} \geq 10.8$ m s^{-1}, (SST ≤ 8 °C)	0.59	0.95	0.06	0.11	0.11

[a] The definitions of the verification scores Percent Correct (PC), Bias ratio (BIASr), Equitable Threat Score (ETS), Heidke Skill Score (HSS), and Peirce Skill Score (PSS) for a 2 × 2 contingency table with predictions and observations are provided e.g. by Wilks (2011) (Ch. 8).

criterion of the ISO 19906 uses a threshold for the wind speed of $10\,m\,s^{-1}$, but is otherwise similar to the Mertins (1968) criterion. However, there are no observations in the control data set with a sea-surface temperature above 8 °C, so the test is only valid for those areas and situations with an SST below this value. When applying such a combination of thresholds for both wind speed and temperature instead of only a single temperature threshold, the verification scores are more accurate with a percent correct above 50% (Table 5). However, although the PC and BIASr scores are more accurate than the single upper-air parameter method of T_{850} of the Japanese and Russian studies, the values of the equitable scores (ETS, HSS, and PSS) in these two models are in the same ranges. The equitable scores of this model is also quite far from the scores of the combined sets of the upper-air parameters (ΔT_{850}, T_{850} with or without V_{850}).

5.3. Other variables tested

Common parameters applied to categorize cold-air outbreaks or polar low situations are temperature or potential-temperature difference between the sea surface and the air aloft either at 850 hPa, 800 hPa, 700 hPa or 500 hPa (Kolstad et al., 2009; Føre et al., 2011; Papritz et al., 2015; Fletcher et al., 2016). The difference between the surface skin potential temperature and the potential temperature at 850 hPa ($\Theta_{0m} - \Theta_{850}$), and the temperature difference between sea surface and 850 hPa or 500 hPa are also tested as predictors in the logistic regression model. All these variables are significant around certain thresholds when these predictors are applied alone, but are not providing any improvement to the logistic regression model when combining them with other parameters or compared to the combination of T_{850} and ΔT_{850}. In addition, these cold-air outbreak variables are not suited for the CAO_MTW situations. Furthermore, it would have been preferable to include a model with some wave information, since the sea spray from collision between waves and ship is important for icing to occur, particularly near the coast and the ice edge due to fetch limitations when the wind is blowing from the land or sea ice (Samuelsen, 2018). However, medium-range predictions of significant wave height are less accurate than the upper-air parameters from the atmosphere. In the verification of the reanalysis data the accuracy of the significant wave height was good with a BIAS near 0 m and a mean absolute error not more than 1 m (Table 4). However, when applying a dichotomized H_s in combination with the other predictors of the upper-air parameters, the logistic regression model is not improved. A user of this simplified model with upper-air parameters alone must therefore be made aware of this shortcoming of not applying wave information for water availability when applying the model near the ice edge.

6. Summary and conclusions

This study contains almost 1,600 icing and no-icing events in the sea areas around Northern Norway and the Svalbard archipelago from 17 different medium-sized and large-sized ships. The results are divided into three parts: Firstly, investigation of the most important parameters observed in icing compared to no-icing events. Secondly, an overview of the main large-scale weather situations arising in icing and no-icing events represented by map composites, vertical cross sections, and vertical profiles. Finally, a simple model is developed based on upper-air parameters for medium-range prediction of icing potential.

As highlighted from the results of the current study, higher waves, and stronger winds are important for icing to be encountered when the temperatures are below 0 °C. Low air temperatures are important together with high waves and strong winds, but low temperatures do not alone increase the risk of icing compared to higher temperatures as long as the temperature is below the freezing point of fresh water. Low sea-surface temperatures do clearly not indicate a higher risk of icing as long as the SSTs in general are below 0 °C. This apparent contradictory result stems from the fact that other factors like wave height and the presence of showers are more important than SST in order to induce icing. This contradicts some arguments from previous studies emphasizing the importance of low SST for icing or more severe icing rates to be encountered (DeAngelis, 1974; Overland et al., 1986; Overland, 1990). The results of the current study also follow up the results of a verification study of icing rates (Samuelsen, 2018) regarding non-meteorological factors like mean speed of vessel and heading, i.e. that heading angle is a more important factor than vessel speed for icing. It is namely apparent that the icing events in contrast to the no-icing events do not occur under a significant higher median vessel speed. In addition, the ships in the icing events are significantly headed more towards the wind than are the ships in the no-icing events. Moreover, the results indicate that sea-spray icing with or without snow is the most common cause of icing in the Barents Sea, the Greenland Sea, and the Norwegian Sea. Icing may also ensue due to evaporation fog or sea smoke, but mainly in conjunction with sea spray. Furthermore, the results state that freezing rain rarely occurs in conjunction with icing in these areas. However, discrimination of icing cause based on the icing-cause code alone, must be applied with caution.

Furthermore, it is found that the most common large-scale weather situation in icing events in these areas is during a northerly flow entitled cold-air outbreak from the ice (CAO_ICE). This is quite different from the observed climatology of a previous study of Vasilyeva, (1971) in which most events occurred during southerly flows, i.e. in cold-air outbreak mountain-wave conditions (CAO_MTW) outside the mainland of Northern Norway or Russia. In addition, in the current study most icing events arise with a temperature at 850 hPa lower than −11 °C. This is a considerable higher value than the threshold of −18 °C suggested by the Japanese and Russian studies in the 1960s and 1970s in the seas around Japan and eastern Russia (Sawada, 1967; Sawada, 1968; Vasilyeva, 1971; Borisenkov and Pchelko, 1975). A typical pattern in these CAO_ICE situations is a low pressure system situated in the southeastern part of the Barents Sea in conjunction with higher pressure in the Norwegian Sea or Greenland Sea setting up a strong northerly or northeasterly wind field in the area between the pressure anomalies. However, icing may in some circumstances also occur in CAO_MTW conditions either due to southerly boras from the land areas of Northern Norway, or on the west side of Spitsbergen during easterly flow. In rare circumstances icing does also occur in northwesterly flow on the east side of Spitsbergen. As a whole, the main difference between the CAO_ICE and the CAO_MTW events is the stronger stratification in the CAO_MTW scenario due to Föhn adiabatic warming on the lee-side of the barriers compared to the more terrain-undisturbed flow from the ice in the CAO_ICE scenario.

Next, it is demonstrated that the risk of icing, mostly spray icing, is higher when snow is observed, either as showers or as frontal precipitation. This finding is supported by cloud-cover and relative-humidity observations. The presence of snow will lead to higher relative humidity compared to a situation without precipitation. The higher risk of icing associated with low compared to high relative-humidity situations, is due to a potentially stronger evaporative and radiative heat flux in the low R_H-cases. This is counteracted when snow is present. In fact, the strong association between relative humidity and the presence of snow implies that relative humidity is only a significant covariate in the logistic-regression model applied in the current study when the presence of snow is included as a separate covariate. The importance of the presence of showers and fronts during icing is particularly apparent in the cold-air outbreaks from the ice and the cold-air outbreak mountain-wave situations on the west side of Spitsbergen. However, it cannot be concluded whether the precipitation in itself or the wind gusts and turbulence associated with these phenomena are the most important factors. Both circumstances may have influence; the former in increasing the amount of water available for freezing and raising the freezing temperature of the brine water on the ship compared to a situation without precipitation, and the latter by increasing the convective and evaporative heat flux due to stronger mixing taking place in

a more turbulent environment relative to less turbulent conditions. Although earlier studies have pinpointed the possible importance of solid precipitation in conjunction with icing (Brown and Agnew, 1985; Horjen, 1990; Samuelsen et al., 2017)), this is the first time the association between observed icing/no-icing events and observed snow events has been formally tested.

A medium-range prediction model for icing potential is suggested. The model is based on a combination of criteria of $T_{850} \leq -15\,^{\circ}\mathrm{C}$ and $\Delta T_{850} \leq -4.0\,^{\circ}\mathrm{C}$. This might give an indication of possible icing potential 16–23 days ahead. For somewhat shorter lead times adding a criterion of $V_{850} \geq 8\,\mathrm{m\,s^{-1}}$ might give even more accurate results. Thus, this study underlines the potential of applying upper-air parameters in order to provide more accurate icing forecasts compared to traditional icing predictions based on surface parameters alone. Icing-forecasting models using T_{850} have not been proposed in icing research or forecasting in the last 40–50 years when development in forecasting models have had high priority. However, still more verification studies are needed of the proposed icing model based on forecast variables calculated for longer lead times in order to finally determine the accuracy of the model for medium-range icing prediction.

If knowledge of sea-ice conditions is added with a high degree of accuracy to such models, it might be possible to remove areas with strong fetch limitation in the predictions of icing potential. However, for predictions in a shorter perspective of a couple of days, it is probably preferable to apply more accurate and advanced modelling procedures calculating the degree of icing based on available spray flux and heat fluxes based on surface parameters for particular ship types as was the use for the model of Samuelsen et al. (2017).

Finally, it is important to bear in mind that vessels or structures that have very different bow shapes, free-boards, or are exposed to icing at completely different elevations, might experience icing under different conditions than the ships of the current study. The results presented here may therefore not be valid in general for all ships. However, gaining more information about solid precipitation, turbulence, and sea-spray under offshore conditions in conjunction with most relevant atmospheric and oceanographic parameters for fixed ship types, is a way in bridging the gap between the current knowledge stages. Only time will tell whether a diligent observational program on several fixed ships over long time periods providing observations from a vast amount of parameters is economically and practically feasible. This may ultimately lead to development of models that provide forecasts for all relevant ship types and other offshore installations.

Conflict of interest

None.

Funding

This work was supported by Norwegian Research Council through the MAROFF program [grant number 226404].

Acknowledgements

The authors would like to thank all colleagues at UiT The Arctic University of Norway, and collaboration partners at the Norwegian Meteorological Institute for providing crucial help, feedback and discussions. The Norwegian deep water program is acknowledged for providing the NORA10 hindcast data. The Open Geospatial Consortium (OGC) is acknowledged for the application of some weather symbology elements in Fig. 5. In addition, we thank the Department manager M. N. Jørgensen of the Norwegian Coast Guard (pers. comm., April 2014) for allowing publication of the observations from the coast guard ships. A special gratitude goes to Dr Heiko Klein for helping out with the derivation of the NORA10 data. Gratitude is also provided to the reviewers for fruitful feedbacks and comments which have increased the quality of the manuscript. Finally, the authors would like to thank Associate Professor Kåre Edvardsen for encouraging discussions and feedbacks of the manuscript.

Appendix A. Supporting information

Supporting information to this article can be found online at https://doi.org/10.1016/j.wace.2019.100200.

References

Borisenkov, Y.P., Panov, V.V., 1972. Osnovnyye rezultaty i perspektivy issledovaniy gidrometeorologicheskikh usloviy obledeneniya sudov (Primary results and prospects for the investigation of the hydrometeorological conditions of ship icing). Technical Report Trudy No. 298, Arkticheskii i Antarkticheskii Nauchnolssledovatiel'Skii Institut. Gidrometeoizdat, Leningrad.

Borisenkov, Y.P., Pchelko, I.G., 1975. Indicators for forecasting ship icing. Cold Regions Research and Engineering Laboratory, Hanover, New Hampshire, USA Technical report TL 481.

Brown, R.D., Agnew, T., 1985. Characteristics of marine icing in Canadian waters. In: Proceedings of the International Workshop on Offshore Winds and Icing, pp. 78–94.

Brown, R.D., Roebber, P., 1985. The Ice Accretion Problem in Canadian Waters Related to Offshore Energy and Transportation. Candian Climate Centre, Atmospheric Environment Service Technical Report 85–13.

Buizza, R., Leutbecher, M., 2015. The forecast skill horizon. Q. J. R. Meteorol. Soc. 141 (693), 3366–3382. ISSN 1477-870X. https://doi.org/10.1002/qj.2619.

Chambers, J.M., Cleveland, W.S., Kleiner, B., Tukey, P.A., 1983. Graphical methods for data analysis. Wadsworth International Group, Belmont, California ISBN 0871504138.

DeAngelis, R.M., 1974. Superstructure icing. Mariners Weather Log 18. Nacional Oceanic and Atmospheric Administration (NOAA), Washington D.C.

Dee, D.P., Uppala, S.M., Simmons, A.J., Berrisford, P., Poli, P., co-authors, 2011. The ERA-Interim reanalysis: configuration and performance of the data assimilation system. Q. J. R. Meteorol. Soc. 137 (656), 553–597. https://doi.org/10.1002/qj.828.

Durran, D.R., 1990. Mountain waves and downslope winds. In: Atmospheric processes over complex terrain. Springer, pp. 59–81. https://doi.org/10.1175/JCLI-D-15-0268.1.

Fletcher, J., Mason, S., Jakob, C., 2016. The climatology, meteorology, and boundary layer structure of marine cold air outbreaks in both hemispheres. J. Clim. 29 (6), 1999–2014. https://doi.org/10.1175/JCLI-D-15-0268.1.

Føre, I., Kristjánsson, J.E., Saetra, Ø., Breivik, Ø., Røsting, B., 2011. The full life cycle of a polar low over the Norwegian Sea observed by three research aircraft flights. Q. J. R. Meteorol. Soc. 137 (660), 1659–1673. ISSN 1477-870X. https://doi.org/10.1002/qj.825.

Furevik, B.R., Haakenstad, H., 2012. Near-surface marine wind profiles from rawinsonde and NORA10 hindcast. J. Geophys. Res.: Atmosphere 117 (D23) ISSN 2156-2202. https://doi.org/10.1029/2012JD018523.D23106.

Gaberšek, S., Durran, D.R., 2004. Gap flows through idealized topography. Part I: Forcing by large-scale winds in the nonrotating limit. J. Atmos. Sci. 61 (23), 2846–2862. https://doi.org/10.1175/JAS-3340.1.

Haiden, T., Janousek, M., Bidlot, J., Ferranti, L., Prates, F., co-authors, 2016. Evaluation of ECMWF forecasts, including the 2016 resolution upgrade. Technical Memorandum 792. ECMWF - European Centre for Medium-Range Weather Forecasts.

Horjen, I., 1990. Numerical modelling of time-dependent marine icing, anti-icing and de-icing. NTH - Norges Tekniske Høgskole Doctoral thesis.

International Organization for Standardization (ISO), 2010. ISO 19906: Petroleum and natural gas industries - Arctic offshore structures.

Jurčec, V., 1980. On mesoscale characteristics of bora conditions in Yugoslavia. Pure Appl. Geophys. 119 (3), 640–657. ISSN 1420-9136. https://doi.org/10.1007/BF00878165.

Kolstad, E.W., Bracegirdle, T.J., Seierstad, I.A., 2009. Marine cold-air outbreaks in the North Atlantic: temporal distribution and associations with large-scale atmospheric circulation. Clim. Dyn. 33 (2–3), 187–197. https://doi.org/10.1007/s00382-008-0431-5.

Kolstad, E.W., 2011. A global climatology of favourable conditions for polar lows. Q. J. R. Meteorol. Soc. 137 (660), 1749–1761. ISSN 1477-870X. https://doi.org/10.1002/qj.888.

Kolstad, E.W., 2017. Higher ocean surface wind speeds during marine cold air outbreaks. In: Quarterly Journal of the Royal Meteorological Society, https://doi.org/10.1002/qj.3068.

Kovrova, A.M., Korotun, C.P., Panov, V.V., 1969. Gidrometeorologicheskiye usloviya obledeneniya na sudakh v arkticheskikh moryakh. (Hydrometeorological conditions of icing on ships in the Arctic seasa). Arkticheskii i Antarkticheskii Nauchno-lssledovatiel'skii Institut, Leningrad Technical report.

Kulyakhtin, A., 2014. Numerical Modelling and Experiments on Sea Spray Icing. PhD thesis NTNU - Norwegian University of Science and Technology Available online at: http://hdl.handle.net/11250/277036, Accessed date: 29 June 2017.

Løset, S., Shkinek, K.N., Gudmestad, O.T., Høyland, K.V., 2006. Icing in the Ocean. In: Actions from ice on arctic offshore and coastal structures. Student's Books for Institutes of Higher Education. Special Literature, St. Petersburg (chapter 6), pp. 191–206. LAN.

Lozowski, E.P., Szilder, K., Makkonen, L., 2000. Computer simulation of marine ice

accretion. Philos. Trans. R. Soc. London, Ser. A: Math. Phys. Eng. Sci. 358 (1776), 2811–2845. https://doi.org/10.1098/rsta.2000.0687.
Lundqvist, J., Udin, I., 1977. Ice accretion on ships with special emphasis on Baltic conditions. Research Report 23, Winter Navigation Research Board, Swedish Administration of Shipping and Navigation. Finnish Board of Navigation, Norrköping, Sweden.
Markowski, P., Richardson, Y., 2011. Mesoscale meteorology in midlatitudes, vol. 2 John Wiley & Sonshttps://doi.org/10.1002/9780470682104.
Mertins, H.O., 1968. Icing on fishing vessels due to spray. Mar. Obs. 38 (221), 128–130.
Minsk, L.D., 1977. Ice accumulation on ocean structures. Technical report. In: Cold Regions Research and Engineering Lab.
Norwegian Maritime Authority, 2014. Ulykkesdatabase (Database of ship incidents). Available online at: https://www.sjofartsdir.no/ulykker-sikkerhet/ulykkesstatistikk/datauttrekk/, Accessed date: 29 August 2016.
Norwegian Meteorological Institute, 2016. eKlima - Free access to weather- and climate data from Norwegian Meteorological Institute from historical data to real time observations. Electronic. http://eklima.met.no, Accessed date: 23 June 2016.
Olafsson, H., Eliasson, A.J., Thorsteins, E., 2002. Orographic influence on wet snow icing – Part II: Downstream of mountains. In: Proceedings of the Tenth International Workshop on Atmospheric Icing of Structures (IWAIS), Brno, Czech Republic.
Overland, J.E., 1990. Prediction of vessel icing for near-freezing sea temperatures. Weather Forecast. 5, 62–77. https://doi.org/10.1175/1520-0434(1990)005<0062:POVIFN>2.0.CO;2.
Overland, J.E., Pease, C.H., Preisendorfer, R.W., Comiskey, A.L., 1986. Prediction of vessel icing. J. Clim. Appl. Meteorol. 25 (12), 1793–1806. https://doi.org/10.1175/1520-0450(1986)025<1793:POVI>2.0.CO;2.
Papritz, L., Spengler, T., 2017. A lagrangian climatology of wintertime cold air outbreaks in the irminger and nordic seas and their role in shaping airsea heat fluxes. J. Clim. 30 (8), 2717–2737. https://doi.org/10.1175/JCLI-D-16-0605.1.
Papritz, L., Pfahl, S., Sodemann, H., Wernli, H., 2015. A climatology of cold air outbreaks and their impact on air–sea heat fluxes in the high-latitude South Pacific. J. Clim. 28 (1), 342–364. https://doi.org/10.1175/JCLI-D-14-00482.1.
Reistad, M., Breivik, Ø., Haakenstad, H., Aarnes, O.J., Furevik, B.R., 2011. A high-resolution hindcast of wind and waves for the North Sea, the Norwegian Sea, and the Barents Sea. J. Geophys. Res.: Oceans (C5), 116. 1978–2012. https://doi.org/10.1029/2010JC006402.
Richardson, D., Bidlot, J.-R., Haiden, T., Hewson, T., Janousek, M., co-authors, 2013. Evaluation of ECMWF forecasts, including 2012-2013 upgrades. Technical Memorandum 710, ECMWF - European Centre for Medium-Range Weather Forecasting.
Samuelsen, E.M., 2007. Et dynamisk studium av stormen Narve - et kaldluftsutbrudd i Finnmark - ved hjelp av observasjoner og numeriske simuleringer. (A dynamical study of the storm Narve - a cold air outbreak in Finnmark - with the use of observations and numerical simulations). Master's thesis, University of Bergen, Bergen Available online at: http://hdl.handle.net/1956/17137, Accessed date: 5 March 2018.
Samuelsen, E.M., 2018. Ship-icing prediction methods applied in operational weather forecasting. Q. J. R. Meteorol. Soc. 144 (710), 13–33. ISSN 1477-870X. URL. https://doi.org/10.1002/qj.3174.
Samuelsen, E.M., Løset, S., Edvardsen, K., 2015. Marine icing observed on KV Nordkapp during a cold air outbreak with a developing polar low in the Barents Sea. In: Proceedings of the 23rd International Conference on Port and Ocean Engineering under Arctic Conditions, vol. 87. Norwegian University of Science and Technology, Trondheim, pp. 1–14. Available online at: http://www.poac.com/Papers/2015/pdf/poac15Final00087.pdf, Accessed date: 29 June 2017.
Samuelsen, E.M., Edvardsen, K., Graversen, R.G., 2017. Modelled and observed sea-spray icing in Arctic-Norwegian waters. Cold Reg. Sci. Technol. 134, 54–81. ISSN 0165-232X. https://doi.org/10.1016/j.coldregions.2016.11.002. http://www.sciencedirect.com/science/article/pii/S0165232X16303275.
Sawada, T., 1962. Icing on ships and the forecasting method. Snow and Ice (24), 12–14 (In Japanese).
Sawada, T., 1967. A forecasting method for ship icing near the Kuril Islands (In Japanese). J. Met. lies., JMA 18.
Sawada, T., 1968. Ice accretion on ships in northern seas of Japan. J. Meteorol. Soc. Japan 46, 350–354.
Shekhtman, A.N., 1971. The probability and intensity of the icing-up of ocean-going vessels. DTIC Document Technical report.
Shellard, H.C., 1974. The meteorological aspects of ice accretion on ships. Technical Report 10, World Meteorological Organization. Marine Science Affairs Report.
Skeie, P., Grønås, S., 2000. Strongly stratified easterly flows across Spitsbergen. Tellus 52 (5), 473–486. ISSN 1600-0870. https://doi.org/10.1034/j.1600-0870.2000.01075.x.
Stallabrass, J.R., 1980. Trawler icing - A compilation of work done at N.R.C. Mechanical Engineering Report MD-56. National Research Council Canada.
Stallabrass, J.R., 1971. Meteorological and oceanographic aspects of trawler icing off the Canadian east coast. Mar. Obs. 41 (233), 107–121.
The Wamdi Group, 1988. The WAM ModelA Third Generation Ocean Wave Prediction Model. J. Phys. Oceanogr. 18 (12), 1775–1810. https://doi.org/10.1175/1520-0485(1988)018<1775:TWMTGO>2.0.CO;2.
Undén, P., Rontu, L., Järvinen, H., Lynch, P., Calvo, J., Cats, G., 2011. Coauthors, 2002: HIRLAM-5 scientific documentation. Scientific documentation. Swedish Meteorological and Hydrological Institute (SMHI), Norrköping, Sweden.
Uppala, S.M., Kållberg, P.W., Simmons, A.J., Andrae, U., Bechtold, V.D.C., co-authors, 2005. The ERA-40 re-analysis. Q. J. R. Meteorol. Soc. 131 (612), 2961–3012. https://doi.org/10.1256/qj.04.176.
Vasilyeva, G.V., 1971. Gidrometeorologicheskiye usloviya obledeniya morskikh sudov. (Hydrometeorological conditions of the icing of sea-going ships.). T. Vyp, vol. 87 Gidromet. Nauo-Issled. Centre SSSR, Leningrad.
Vittinghoff, E., Glidden, D.V., Shiboski, S.C., McCulloch, C.E., 2011. Regression methods in biostatistics: linear, logistic, survival, and repeated measures models. Springer Science & Business Mediahttps://doi.org/10.1007/978-1-4614-1353-0.
Wilks, D.S., 2011. Statistical Methods in the Atmospheric Sciences, vol 100 of International Geophysics Series, third ed. Academic Press9780123850225.
WMO, 2015. Manual on Codes. International on codes. Manual 306. Volume I.1. Part A - Alphanumeric codes., World Meteorological Organization (WMO). Available online at. http://www.wmo.int/pages/prog/www/WMOCodes.html.
Zakrzewski, W.P., 1987. Splashing a ship with collision-generated spray. Cold Reg. Sci. Technol. 14 (1), 65–83. http://www.sciencedirect.com/science/article/pii/0165232X87900450.
Zakrzewski, W.P., Lozowski, E.P., 1989. Soviet marine icing data. Canadian Climate Centre, Atmospheric Environment Service Technical report.